

Ultrastructure of dragonfly wing veins: composite structure of fibrous material supplemented by resilin

Esther Appel,¹ Lars Heepe,¹ Chung-Ping Lin^{2,3} and Stanislav N. Gorb¹

¹Functional Morphology and Biomechanics, Zoological Institute, Kiel University, Kiel, Germany

²Department of Life Science, Tunghai University, Taichung, Taiwan

³Department of Life Science, National Taiwan Normal University, Taipei, Taiwan

Abstract

Dragonflies count among the most skilful of the flying insects. Their exceptional aerodynamic performance has been the subject of various studies. Morphological and kinematic investigations have showed that dragonfly wings, though being rather stiff, are able to undergo passive deformation during flight, thereby improving the aerodynamic performance. Resilin, a rubber-like protein, has been suggested to be a key component in insect wing flexibility and deformation in response to aerodynamic loads, and has been reported in various arthropod locomotor systems. It has already been found in wing vein joints, connecting longitudinal veins to cross veins, and was shown to endow the dragonfly wing with chordwise flexibility, thereby most likely influencing the dragonfly's flight performance. The present study revealed that resilin is not only present in wing vein joints, but also in the internal cuticle layers of veins in wings of *Sympetrum vulgatum* (SV) and *Matrona basilaris basilaris* (MBB). Combined with other structural features of wing veins, such as number and thickness of cuticle layers, material composition, and cross-sectional shape, resilin most probably has an effect on the vein's material properties and the degree of elastic deformations. In order to elucidate the wing vein ultrastructure and the exact localisation of resilin in the internal layers of the vein cuticle, the approaches of bright-field light microscopy, wide-field fluorescence microscopy, confocal laser-scanning microscopy, scanning electron microscopy and transmission electron microscopy were combined. Wing veins were shown to consist of up to six different cuticle layers and a single row of underlying epidermal cells. In wing veins of MBB, the latter are densely packed with light-scattering spheres, previously shown to produce structural colours in the form of quasiordered arrays. Longitudinal and cross veins differ significantly in relative thickness of exo- and endocuticle, with cross veins showing a much thicker exocuticle. The presence of resilin in the unsclerotised endocuticle suggests its contribution to an increased energy storage and material flexibility, thus to the prevention of vein damage. This is especially important in the highly stressed longitudinal veins, which have much lower possibility to yield to applied loads with the aid of vein joints, as the cross veins do. These results may be relevant not only for biologists, but may also contribute to optimise the design of micro-air vehicles.

Key words: cuticle; insect; material; morphology; Odonata; structural colouration; wing.

Introduction

Dragonflies and damselflies propel themselves through the air at speeds of partly more than 10 m s^{-1} , and show an exceptional high lift production and manoeuvrability (Nachtigall, 1977; Azuma & Watanabe, 1988; Rüppele, 1989;

Okamoto et al. 1996; Wakeling & Ellington, 1997). Their flight performance has been the subject of various aerodynamic, kinematic and morphological studies (Wootton, 1981, 1991; Newman, 1982; Rüppele, 1989; Vargas et al. 2008; Wootton & Newman, 2008; Kim et al. 2009; Jongerius & Lentink, 2010). As in all winged insects, their wings lack internal muscles and, thus, deform passively during flight, driven by aerodynamic but mainly by inertial forces (Wootton, 1981, 1991; Newman, 1982; Wootton & Newman, 2008; Jongerius & Lentink, 2010). As members of the extant Paleoptera, Odonata do not have the ability to fold their wings (Kukalová-Peck, 1974; Willkommen, 2009), as do the representatives of Neoptera, which are more adapted to terres-

Correspondence

Esther Appel and Stanislav N. Gorb, Functional Morphology and Biomechanics, Zoological Institute, Kiel University, Am Botanischen Garten 1–9, D-24098 Kiel, Germany. E: eappel@zoologie.uni-kiel.de and sgorb@zoologie.uni-kiel.de

Accepted for publication 3 July 2015

trial locomotion. These characteristics of odonate wings are beneficial for the investigation of wing structure and material composition, particularly with respect to flight. Additionally, some recent studies aimed to draw inspiration from their wing design, in order to improve the performance of so-called micro-air vehicles (MAVs). The latter are small autonomous or remotely controlled aircrafts, designed for the reconnaissance in confined and poorly accessible space. Recent studies have shown that the aerodynamic performance of MAVs, such as 'Delfly', which has been equipped with rather slack, sail-like wings, may be improved through structural rigidity imparting veins, which enable directed passive deformations, minimise wing tear and increase the fracture toughness and, thus, the stability of a wing (Wootton, 1981, 1991; Newman, 1982; Wootton & Newman, 2008; Lentink et al. 2009; Zhao et al. 2009; Jongerius & Lentink, 2010; Dirks & Taylor, 2012).

Wings of Odonata are corrugated, showing a three-dimensional network of slender, perpendicularly arranged cross veins, which are connected to thick, longwise running longitudinal veins in the form of wing vein joints. This design provides the odonate wing with strong span-wise and less chord-wise flexural rigidity (Newman, 1982; Wootton, 1991; Combes & Daniel, 2003; Wootton & Newman, 2008). With high-speed analyses, Koehler et al. (2012) examined the occurrence of wing twisting as well as span-wise and chord-wise camber during the stroke cycle of free-flying dragonflies, and showed the span-wise camber being near its peak at stroke reversal, and the chord-wise camber culminating at the beginning of the downstroke. Both chord-wise and small span-wise flexibility in a rather stable or stiff wing, in combination with kinematics, inertia and fluid-structure interactions, were shown to improve the aerodynamic and mechanical performance of a dragonfly or insect wing, which is not possible in completely rigid wings (Combes & Daniel, 2001; Sane, 2003; Vanella et al. 2009; Du & Sun, 2010; Koehler et al. 2012; Stanford et al. 2012; Mountcastle & Combes, 2013). Further studies suggested the increased chord-wise flexibility to be correlated with the presence of resilin-bearing wing vein joints (Gorb, 1999; Appel & Gorb, 2011; Donoughe et al. 2011).

Resilin was originally discovered and analysed in detail by Weis-Fogh (1960, 1961a,b), and later by Andersen & Weis-Fogh (1964). This elastomeric protein stands out for its long-range deformability, coupled with an almost complete elastic recovery (97%; Andersen & Weis-Fogh, 1964; Andersen, 2010). In insect flight systems, resilin was suggested to provide additional flexibility and adjustment to external loads (e.g. Andersen & Weis-Fogh, 1964; Appel & Gorb, 2011; Donoughe et al. 2011), as well as elastic energy storage (Andersen & Weis-Fogh, 1964; Rothschild et al. 1975; Bennet-Clark & Lucey, 1976). In contrast to hydrated resilin, which has a Young's modulus of about 0.1–3.0 MPa, sclerotised cuticle exhibits a relatively high stiffness, with a Young's modulus of up to 20 GPa (Vincent & Wegst, 2004;

Elvin et al. 2005; Peisker et al. 2013). The mechanism of resilin elasticity has been recently suggested to be based on a reversible beta-turn transition in a peptide encoded by exon III (*Drosophila* CG15920 resilin; Qin et al. 2012). The *Drosophila* CG15920 resilin was found to consist of two peptides derived from exons I and III, connected through a chitin-binding segment. During energy input these structural changes in the exon III peptide result in elastic energy conversion with high efficiency. After removing the stress, exon III regions of the protein were supposed to recover, thereby releasing the stored potential energy to the elastic network consisting of the exon I protein. And this, in turn, was assumed to result in elasticity, supporting jumping and flying movements (Qin et al. 2012). In previous studies, resilin was shown to occur, for example, in the cuticle of the prealar arm and wing hinge of locusts (*Schistocerca gregaria* Forsskål, 1775), and in the tendon of the pleura-subalar muscle of various dragonfly species either in the form of 2–5- μm -thick continuous layers, separating thin, on average 0.2- μm -thick chitinous lamellae, or in the form of pure resilin pads (Weis-Fogh, 1960). Both forms were covered with a thin, external epicuticle (Weis-Fogh, 1960).

Insect cuticle is a fibrous composite material mainly composed of chitin microfibrils embedded in a protein matrix. With an estimated stiffness of about 150 GPa (Vincent & Wegst, 2004), chitin microfibrils in combination with proteins may, thus, provide a major contribution to the cuticle stiffness. The direction of their arrangement is specific for the different cuticle layers. Depending on its chemical composition (e.g. tanning), the hydration status, and the presence of resilin, cuticle mechanical properties may range extremely from rather stiff to very soft and flexible (Vincent & Wegst, 2004). By means of electron microscopy, three different cuticle layers in the insect cuticle have been previously described. (i) The outermost epicuticle is very thin and consists of several layers including a wax layer. (ii) The exocuticle is typically tanned, dark, dehydrated and has a Young's modulus of 1–20 GPa (Vincent & Wegst, 2004) with a helicoidal architecture of microfibrils (Banerjee, 1988). (iii) The endocuticle is softer, relatively strong hydrated and less tanned (Young's modulus ranges from 1 kPa to 50 MPa; Vincent & Wegst, 2004). Additionally, some insects have a layer of less sclerotised cuticle between the exo- and endocuticle, called mesocuticle (Neville, 1975; Binnington & Retnakaran, 1991).

Up to now, the ultrastructure of insect wing veins has only been marginally studied (Banerjee, 1988; Chen et al. 2012). As mentioned above, dragonfly wings are notably adapted to flight and their wing vein cuticle is specialised for particular types of mechanical loads, such as bending and torsion. During flight, wing veins have to undergo countless loading-unloading cycles and, as mentioned above, require both stability and flexibility. Studying the morphology and material composition of dragonfly wing veins and the wing membrane may contribute to improve the design of MAVs. Especially, the incorporation of wing

veins has been shown to significantly improve the aerodynamic performance and wing stability of MAVs (Lentink et al. 2009; Zhao et al. 2009; Jongerius & Lentink, 2010; Dirks & Taylor, 2012).

Besides its influence on mechanical stability, insect cuticle is also a source of colouration. Depending on its source, we differentiate between pigmentary colours and structural colours. The former are produced by selective absorption of visible wavelengths by pigment molecules. The latter arise from interference or more generally the physical interactions of light waves with nanostructured elements that vary in refractive index (e.g. Fox, 1976; Parker, 1999; Prum et al. 2005). These nanostructures may lie within or below the cuticle, as well as in cuticular processes like butterfly scales (Veron et al. 1974; Parker, 1999; Vukusic & Sambles, 2003a; Stavenga et al. 2004; Prum et al. 2005). Light scattering can further be classified into incoherent and coherent scattering, dependent on the spatial distribution of the scattering objects (e.g. Prum et al. 1998, 2004). Incoherent light scattering, like Tyndall or Raleigh scattering, occurs when the scatterers are randomly and spatially independent distributed over the spatial scale of visible light wavelengths (Prum et al. 2004). Coherent scattering, in contrast, premisses a spatial periodic distribution of scatterers (Prum et al. 2004). In the former case, scattered light waves have random relative phases in the direction of interest and the phase relationships among scattered light can be ignored, while in the latter, scattered light waves have non-random relative phases in the direction of interest and, thus, structural colouration may be produced by differential reinforcement or interference among the scattered light waves from multiple scattering interfaces (Prum et al. 2004). In the past, coherent light scattering has mostly been associ-

ated with iridescence. Nevertheless, Prum et al. (1998) identified a new class of coherently scattering nanostructures, termed quasiordered arrays that do not produce prominent iridescence. Their findings resulted in the correction of many structural colourations attributed to Tyndall scattering to be actually caused by coherent scattering of quasiordered arrays (Prum et al. 1999; Prum & Torres, 2003a,b; Prum et al. 2004, 2009).

In the present study, the application of: (i) bright-field light microscopy (LM), (ii) wide-field fluorescence microscopy (WFM), (iii) confocal laser-scanning microscopy (CLSM), (iv) scanning electron microscopy (SEM), (v) transmission electron microscopy (TEM), and (vi) spectrometry were combined in order to elucidate the structure and composition of wing vein cuticle, particularly with respect to the distribution of resilin. For this purpose, two odonate species were selected: the calopterygid damselfly *Matrona basilaris basilaris* (MBB; Selys, 1853), with its dark coloured wings and unusually whitish-blue coloured veins; and the libellulid dragonfly *Sympetrum vulgatum* (SV; Linnaeus, 1758), having transparent wings with brownish coloured wing veins.

Materials and methods

Specimens

Specimens of SV were collected in Kiel (Germany) in 2010 and 2011 with the permission of the 'Landesamt für Landwirtschaft, Umwelt und ländliche Räume (Schleswig-Holstein)' (LLUR) and stored at -70°C or used directly for investigations. Specimens of MBB were collected in Taichung (Taiwan) sent (alive) to Kiel and stored at -70°C or used directly for investigations. Fore and hind wings were cut off for microscopic investigations. Right forewings of SV and MBB are shown in Fig. 1A,C.

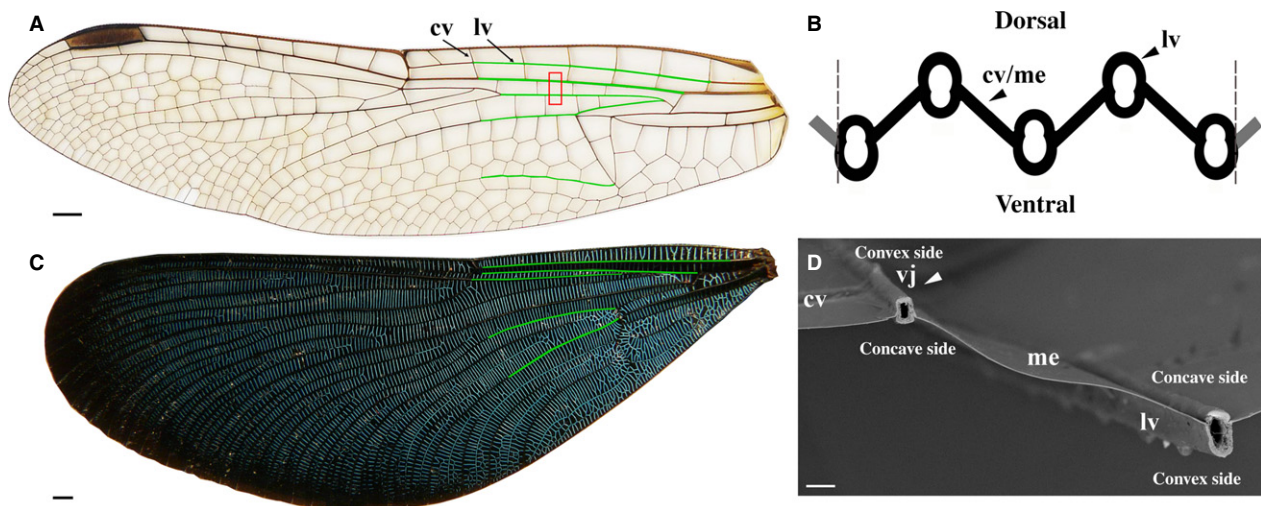


Fig. 1 *Matrona basilaris basilaris* (MBB) and *Sympetrum vulgatum* (SV), wings. (A, C) Photography (reflex camera, Canon EOS 7D), right forewing of SV (A) and MBB (C) shown from the ventral side; examined veins marked in green. (B) Scheme of wing cross-section, showing the corrugated design. (D) SEM, longitudinal vein cross-sections of SV (see red square), showing the concave and convex longitudinal wing vein sides and interconnecting cross vein. cv, cross vein; lv, longitudinal vein; me, wing membrane. Scale bars: 1 mm (A, C); 50 μm (D).

Fluorescence microscopy

Insect cuticle is known for emitting autofluorescences at different wavelengths, depending on the material composition, for example, the degree of sclerotisation and the presence of resilin (e.g. Andersen & Weis-Fogh, 1964; Michels & Gorb, 2012). Due to the two aromatic compounds di- and trityrosine, resilin has an autofluorescence at the narrow band of wavelengths at about 415 nm, when excited with UV-light (Andersen, 1963; Andersen & Weis-Fogh, 1964; Burrows et al. 2008). However, the maximum excitation wavelength of resilin and the fluorescence intensity were shown to be pH-dependent. The maximum excitation wavelength ranges from 285 to 320 nm in acid or alkaline media, respectively, with increased fluorescence intensity in alkaline media (Andersen, 1963). In order to distinguish resilin from other proteins emitting blue autofluorescence when excited with UV-light (Fujimori, 1978; Garcia-Castineiras et al. 1978; Gast & Lee, 1978), additional analyses, for example, staining by toluidine blue, TEM analyses showing its amorphousness, stress birefringence, swelling in aqueous media or mechanical tests, are necessary (see also Michels & Gorb, 2012). In contrast to resilin, insect cuticle shows a strong autofluorescence at wavelengths ranging from blue-green to deep-red (Michels & Gorb, 2012).

For WFM and CLSM, wings were briefly placed into 70% ethanol and washed in distilled water. Vein cross-sections of up to 5 mm thickness were produced with a razor blade, mounted in glycerine on a glass slide, and covered with a cover slip. For WFM, a fluorescence microscope (Zeiss Axioplan, Germany) was equipped with the following filter sets: DAPI-filter set (excitation 321–378, FT395, BP420–470 nm), UV-filter set (365/12, FT395, LP397 nm), blue filter set (450–490, FT510, LP520 nm), green filter set (545/25, FT570, LP590 nm). The CLSM Zeiss LSM 700 (Carl Zeiss Microscopy GmbH) was equipped with the following four lasers: 405, 488, 555 and 639 nm. For emission detection, the following emission filters were used: BP420–480, LP490, LP560 and LP640 nm. Although Andersen (1963) showed an excitation maximum of resilin at 320 nm (at alkaline pH), Michels & Gorb (2012) demonstrated that the application of a 405-nm laser, together with the aforementioned bandpass filter, is appropriate to visualise and analyse the presence and distribution of resilin in the arthropod exoskeleton.

Maximum intensity projections were subsequently created based on the collected image stacks by using the ZEN 2008 software (light edition, freeware). The CLSM was equipped with a black-and-white camera, so that colours were assigned to the laser lines used afterwards.

SEM

For SEM, wings were air-dried or frozen in liquid nitrogen or at -140°C in the cryo-preparation prechamber of the microscope. For these analyses, the proximal part of wings of both species was analysed. Five longitudinal (MA, MP, RA, RP and the ScP vein) and five cross veins attached to each longitudinal vein in the proximal wing part of each studied individual were examined. Each longitudinal vein was fractured on three sides in the area shown in Fig. 1. In sum, five individuals of every species and for every technique were examined. Measurements were taken on 10 sites of each cross-section. The side of fracture was chosen to be only a few millimetres up to 1 cm away from the vein section used for CLSM. The wing sections were mounted on a holder with carbon Leit-tabs (Plano GmbH, Wetzlar, Germany) and Leit-C conductive carbon cement (Neubauer, Münster, Germany) for the analysis at room temperature

or with Tissue-Tek O.C.T. compound (Sakura Finetek Europe B.V., Zoeterwoude, The Netherlands) for the analysis at -120°C (Cryo-mode). Specimens were sputter-coated with gold-palladium (6–10 nm thickness) using a Leica EM SCD 500 High-Vacuum Sputter Coater (Leica Microsystems GmbH, Wetzlar, Germany) or with the internal sputter coater of the microscope, and examined in a Hitachi S-4800 SEM (Hitachi High-Tech., Tokyo, Japan), equipped with a Gatan ALTO 2500 cryo-preparation system (Gatan, Abingdon, UK), at an accelerating voltage of 3 kV.

The images were analysed with the aid of the software Adobe Photoshop (version CS5; Adobe Systems, Germany). The number of different cuticle layers was counted and their thickness was measured on five sides on both the convex and the concave side of each vein cross-section. Differentiation between different cuticle layers followed the characteristics of single layers described in 'Electron Microscopy'. Proportional values of every single cuticle layer were determined for each vein by normalisation to the respective total cuticle thickness of the vein examined. These data were used in statistical analyses.

TEM and bright-field LM

For bright-field LM and TEM, wing sections with dimensions of about 0.5×0.5 cm were fixed in a solution of 2.5% glutaraldehyde in $1 \times$ (pH 7.4) phosphate-buffered saline (PBS) for 8–12 h at 4°C , washed three times in $1 \times$ PBS each for 20 min and once in double-distilled water for 10 min at 4°C , fixed in 1% aqueous OsO_4 for 1 h at 4°C (not for the embedding in Lowicryl HM20), and washed three times in double-distilled water, each time for 20 min. Afterwards, they were dehydrated in an ethanol series of 30–100% at 4°C , infiltrated with Epon/ethanol or Lowicryl HM20/ethanol mixtures, and subsequently embedded in Epon 812 (Glycidether 100; Carl Roth GmbH, Karlsruhe, Germany) and Lowicryl HM20 (Monos-tep; Polysciences, Warrington, PA, USA). Specimens in Epon were polymerised at 60°C for 48 h. Specimens in Lowicryl HM20 were polymerised under UV-light (366 nm) for 24–48 h and afterwards exposed to daylight for 1–2 days with open lid to complete polymerisation. Specimens were cut into semi-thin sections of 1–3 μm thickness for LM and in ultrathin sections of 50–80 nm thickness for TEM with a Leica EM UC7 ultramicrotome (Leica Microsystems GmbH).

For LM, Epon-embedded sections were treated with a mixture of KOH, methyl alcohol and propylene oxide (Maxwell, 1978) for 8–15 min and washed in running water for 5–10 min. Subsequently, sections were stained with toluidine blue, Cason's triple stain, Heidenhain's azan stain or Nile blue, subsequently mounted in glycerine, and inspected right after the staining and after 24 h, 48 h and 72 h. Prior to staining, sections of wing veins of MBB were treated with a solution of 3% hydrogen peroxide, 0.5% KOH and 1% Na_2HPO_4 , neutralised in 1% acetic acid, and rinsed in water to bleach the pigments. For toluidine blue staining, sections were incubated with 0.1–0.5% toluidine blue (in an aqueous solution of 1% sodium tetraborate) for 30–60 s and destained using a stream of tap water.

Cason's staining solution consists of 1 g phosphotungstic acid, 2 g orange G, 1 g aniline blue and 3 g acid fuchsine, dissolved in 200 mL distilled water (Cason, 1950), and was applied for 5 min. Sections were subsequently rinsed with 5% acetic acid and 100% EtOH.

Heidenhain's azan staining was conducted using the following protocol, partly adopted from the one by Romeis (1989, 2010): sections were incubated in a preheated solution of 0.1 g azocarmine

G, 100 mL distilled water and 1 mL 100% acetic acid for 20 min, subsequently bathed in an aniline solution (0.1 mL aniline and 100 mL 90% EtOH) for 15 min, transferred into an acetic acid–ethanol solution (100 mL 96% EtOH and 1 mL acetic acid) for 1 min, incubated in 5% phosphotungstic acid for 2–3 h, rinsed in distilled water, and bathed in a solution of 0.5 g aniline blue, 2 g orange G, 100 mL distilled water and 8 mL 100% acetic acid for 2–3 h, and finally rinsed twice in distilled water.

Nile blue staining was conducted partly based on the protocol by Pearse (1964) and Romeis (2010). Bleached sections were incubated in a saturated solution of Nile blue in 1% sulphuric acid and rinsed in distilled water for the visualisation of both lipofuscins and melanins, or quickly rinsed in 1% sulphuric acid and rinsed four times in acetone for each 15 s for the visualisation of only melanins.

For TEM, sections were post-stained with a saturated aqueous solution of uranyl acetate for 15 min, and with lead citrate for 5 or 10 min. The stained sections were examined using a Philips CM10 TEM (Philips Scientifics, Eindhoven, The Netherlands) at an accelerating voltage of 80 kV.

Spectrometry

The reflectance spectra measurements were performed with a high-resolution fibre optic spectrometer (HR4000; Ocean Optics, Dunedin, FL, USA), equipped with a DH-2000-BAL light source (Ocean Optics) and a fibre optic probe, including the 400 µm detector and the light source. The spectrum was measured with normal incident light at 1 and 5 mm distance from the sample by using the Spectra Suite software (Ocean Optics). Signal averaging and boxcar averaging were used to improve the signal-to-noise ratio and the amplitude resolution. Signal averaging is done by averaging a number of individual full scans and was set to 15. Boxcar averaging averages a number of pixel values (boxcar width) on each side of a given pixel. Here, the boxcar width was set to 5. The integration time was set to either 620 ms in the case of a distance of 1 mm to the specimen and to 4200 ms in the case of 5 mm distance. Before starting the measurements, the spectrometer was calibrated with a white standard (WS-1-SS; Ocean Optics). For recording a dark reference spectrum, the shutter was closed and the detector screened from light. For reflectance measurements, whitish-blue coloured wing veins were cut out and tightly arranged to each other. For each sample, five separate measurements were taken.

Statistical analyses

The data obtained for the single cuticle layer thicknesses were used for two different purposes. First, the data were compared for longitudinal veins, cross veins and the wing membrane, and between the convex side and concave side of longitudinal veins of the same species. Second, the data were compared between the two odonate species examined. These two analyses were performed with the Mann–Whitney rank sum test. All statistical analyses were performed with Sigmaplot software (version 12.5, 2013).

Results

Wings of Odonata show a corrugated wing design with longitudinal veins situated on the fold tips of a zigzag-like wing profile (Fig. 1B,D). Cross veins interconnect longitudinal veins and are joined to the latter in the form of vein

joints (Fig. 1D). Depending on which side of the longitudinal vein is examined, the concave side, situated on the fold's valley side, and the convex side, situated on its hill side, were differentiated between (Fig. 1D).

By examining dragonfly wing vein cross-sections under a fluorescent microscope equipped with an UV-filter set (see Materials and methods), it was found that the inner part of the cuticle showed a strong blue autofluorescence. Such an autofluorescence at a narrow band of wavelengths at about 415 nm was previously shown to be one of the criteria suggesting the presence of resilin (Andersen & Weis-Fogh, 1964; Andersen, 2003; see 'Fluorescence microscopy'). Other microscopically examinable criteria include resilin's amorphousness in the electron microscope, and a sapphire blue colour, when stained with toluidine blue. The application of different microscopical techniques supported this initial assumption and, additionally, elucidated the complex organisation of the cuticle consisting of six different cuticle layers and the endocuticle as the main source of the blue autofluorescence.

Organisation of wing vein cuticle

Electron microscopy

The current results suggest that dragonfly and damselfly wing veins consist of up to six different cuticle layers, namely, the epicuticle, the outer exocuticle, the intermediate cuticle or mesocuticle, the undulating exocuticle, the endocuticle and the mixed cuticle (Fig. 2). Thickness and relative thickness of each cuticle layer can be found in Table 1. As already indicated by previous studies, longitudinal veins vary in thickness along the wing span and chord (Jongerijs & Lentink, 2010). Here, results refer only to the proximal part of the wings. For the examination of wing veins of SV and MBB, the proximal parts of the following longitudinal veins, together with respective cross veins, were used (see Fig. 1, green coloured veins): MA, MP, RA, RP and ScP. The following descriptions of single cuticle layers apply for wing veins and the wing membrane of both odonate species studied. Thus, in the following section, thickness will be described by thickness ranges. For medians and percentiles, as well as for the comparison of the species examined, see below and Table 1.

Cuticle layers. Epicuticle. The outermost epicuticle consisted of a prominent wax layer and very thin chitin-lacking, proteinous layers underlying the wax layer (Fig. 2A–C, see *epi* and *wl*). Wings of both species showed continuous wax coverage with wax crystals on wing membrane and wing veins. The epicuticle thickness ranged from about 0.15 to over 0.8 µm, depending on the species and the location on either the wing membrane or vein.

Outer exocuticle. The lamellate outer exocuticle did not show the typical helicoidal arrangement of chitin microfibrils (Banerjee, 1988; Chapman, 1998; Barbakadze et al.

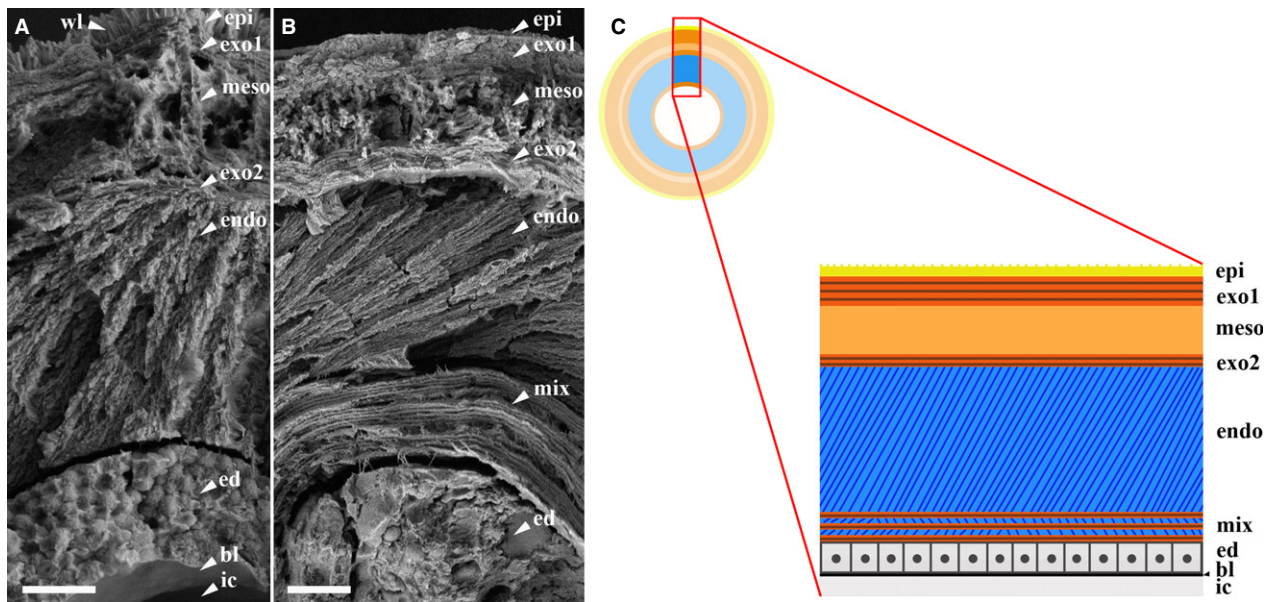


Fig. 2 *Matrona basilaris basilaris* (MBB) and *Sympetrum vulgatum* (SV), wing vein structure. (A, B) SEM, longitudinal vein cross-sections of wings of MBB (A) with five cuticle layers, and of SV with all six possible cuticle layers (B). Epidermal cells of MBB are additionally densely filled with nanospheres. (C) General organisation of the cuticle layers with underlying epidermis and basal lamina. bl, basal lamina; ed, epidermis; endo, endocuticle; epi, epicuticle; exo1, outer exocuticle; exo2, undulating exocuticle; ic, inner cavity; meso, mesocuticle; mix, mixed cuticle; wl, wax layer. Scale bars: 1 μm (A); 2 μm (B).

2006), but a multilayered structure with alternating bright and dark layers (seen in TEM), as already described for the abdominal tergite cuticle of damselflies *Calopteryx virgo* (Linnaeus, 1758) and *C. splendens* (Harris, 1789) (Kuitunen & Gorb, 2011) or the wing membrane of the damselfly *Neurobasis chinensis* (Linnaeus, 1758; Vukusic et al. 2003b; Figs 2A–C and 3A,D, see exo1). Here, the alternating layering was suggested to arise from the difference in distribution of melanin (Vukusic et al. 2003b). The outer exocuticle thickness ranged from about 0.3 μm to over 3.9 μm , depending on the species and localisation in either the wing membrane, longitudinal or cross veins. For median thickness and relative thickness, see Table 1. The outer exocuticle comprised from four to up to 53 bilayers, consisting of one bright and one dark layer. The single bilayers had a thickness from about 0.06 μm up to 2.0 μm .

Mesocuticle. The intermediate cuticle or mesocuticle showed a more spongy structure with rather loosely arranged chitin microfibrils, embedded in a protein matrix, with practically no discernible layering (Figs 2A–C and 3A,D, see meso). Its thickness ranged from 0.2 to 6.9 μm , depending on the species and on the wing structure examined.

Undulating exocuticle. The undulating exocuticle showed the same multilayered structure as already described for the outer exocuticle (Figs 2A–C and 3D, see exo2). Its thickness ranged from about 0.2 μm to up to 1.4 μm and comprised from three to up to eight single layers. The latter had a thickness ranging from about 0.04 μm to up to 0.24 μm .

Endocuticle. The endocuticle consisted of circumferentially arranged chitin-protein microfibrils that were embedded

in a structureless protein matrix (Figs 2A–C and 3A,C,D, see endo). Its thickness ranged from 0.4 μm to up to 16.4 μm , strongly depending on the species and wing structure examined.

Mixed cuticle. The mixed cuticle occurred only rarely, and consisted of alternating layers of exocuticle and endocuticle (Fig. 2B,C, see mix). Its thickness ranged from about 2.4 μm to up to 4.0 μm . The number of the single exocuticle and endocuticle layers ranged from four to up to 10.

Pore channels. Pore channels were found to originate from inner epidermal cells, further penetrate the endocuticle and then cuticle up to the outer exocuticle. In contrast to the endocuticle, where pore channels were found in high numbers and with wide diameters, the undulating cuticle seemed to be a limit, wherefrom pore channels were found rather seldom and being thinner (Fig. 3A,C, see pc).

Epidermal cells and inner cavity. On the inside, the cuticle of longitudinal veins was found to be lined with epidermal cells. In the wings of MBB, the latter were densely filled with spherical nanostructures further called nanospheres (Fig. 4A) and some electron-dense inclusions, probably being pigments (Fig. 4E,F). Nanospheres had a diameter of $0.26 \pm 0.03 \mu\text{m}$ (mean \pm SD), and showed a dark pigmented inner spot and electron transparent outer shell (Fig. 4B,C). The presence of these spherical structures in epidermal cells underlying the cuticle has already been described for abdominal tergites of dragonflies (Veron et al. 1974; Prum et al. 2004). Epidermal cells of wing veins of SV, however, showed no presence of nanospheres (Fig. 4D,G). Only very

Table 1 *Matrona basilaris basilaris* (MBB) and *Sympetrum vulgatum* (SV), cuticle thickness and relative thickness of longitudinal veins, cross veins, and the wing membrane. The total number of individuals of every species examined is five. ca – non-reflecting concave side, ca2 – reflecting concave side ce – convex side, cv – cross vein, lv – longitudinal vein, me – wing membrane.

Cuticle layer	Cross sectional thickness (µm) [median (25th percentile; 75th percentile)]				
	lv				
	ce	ca	ca2	cv	me (ventral, dorsal)
Epicuticle					
<i>S. vulgatum</i>	0.522 (0.421; 0.665)	0.310 (0.265; 0.352)	–	0.258 (0.216; 0.303)	0.198 (0.176; 0.235)
<i>M. b. basilaris</i>	0.342 (0.269; 0.435)	0.379 (0.334; 0.421)	0.192 (0.150; 0.245)	0.252 (0.193; 0.303)	0.226 (0.194; 0.253)
Exocuticle					
<i>S. vulgatum</i>	2.367 (1.873; 2.798)	1.383 (1.249; 1.523)	–	2.533 (2.203; 2.780)	1.747 (1.666; 1.827)
<i>M. b. basilaris</i>	0.587 (0.450; 0.769)	0.530 (0.457; 0.630)	0.645 (0.580; 0.725)	0.789 (0.648; 1.804)	0.580 (0.426; 0.651)
Single bilayer (lv, cv)					
<i>S. vulgatum</i>	0.069 (0.061; 0.080) (lv, cv)				0.027 (0.025; 0.032)
<i>M. b. basilaris</i>	0.078 (0.070; 0.090) (lv, cv)				0.049 (0.046; 0.052)
Mesocuticle					
<i>S. vulgatum</i>	6.104 (5.375; 6.628)	2.026 (1.741; 2.267)	–	–	0.349 (0.316; 0.410)*
<i>M. b. basilaris</i>	2.073 (1.576; 2.611)	1.381 (1.016; 1.701)	0.770 (0.621; 1.025)	0.923 (0.457; 1.210)	0.375 (0.237; 0.436)*
Undulating exocuticle					
<i>S. vulgatum</i>	0.676 (0.446; 0.882)	0.780 (0.558; 0.940)	–	–	–
<i>M. b. basilaris</i>	0.322 (0.244; 0.393)	0.370 (0.303; 0.443)	0.500 (0.295; 0.587)	0.382 (0.295; 0.448)	–
Endocuticle					
<i>S. vulgatum</i>	11.368 (9.855; 14.175)	7.444 (6.286; 9.434)	–	1.271 (0.953; 1.479)	–
<i>M. b. basilaris</i>	8.034 (5.968; 10.680)	5.040 (3.688; 8.699)	1.245 (1.043; 1.677)	1.019 (0.536; 1.525)	–
Mixed cuticle					
<i>S. vulgatum</i>	3.453 (2.962; 3.772)**	2.790 (2.596; 3.030)**	–	–	–
<i>M. b. basilaris</i>	–	–	–	–	–
Cuticle layer	Relative thickness (%) [median (25th percentile; 75th percentile)]				
	lv				
	ce	ca	ca2	cv	me (ventral, dorsal)
Epicuticle					
<i>S. vulgatum</i>	2.397 (1.954; 2.936)	2.315 (2.035; 2.643)	–	6.297 (5.156; 8.300)	9.150 (8.373; 10.045)
<i>M. b. basilaris</i>	3.043 (2.279; 4.250)	4.753 (3.298; 5.824)	5.562 (4.482; 6.476)	6.862 (6.196; 7.967)	22.221 (20.784; 28.408)
Exocuticle					
<i>S. vulgatum</i>	10.436 (9.767; 12.320)	9.904 (8.623; 11.159)	–	63.400 (59.547; 65.857)	82.887 (81.631; 83.563)
<i>M. b. basilaris</i>	5.026 (4.325; 6.642)	6.190 (5.257; 7.853)	19.167 (16.218; 22.709)	29.282 (14.904; 45.759)	58.060 (55.653; 60.144)
Single bilayer (lv, cv)					
<i>S. vulgatum</i>					
<i>M. b. basilaris</i>					
Mesocuticle					
<i>S. vulgatum</i>	27.902 (25.896; 30.238)	14.635 (13.702; 15.549)	–	–	8.159 (7.311; 9.391)
<i>M. b. basilaris</i>	18.133 (15.727; 21.437)	15.390 (12.403; 20.159)	22.249 (17.474; 26.809)	27.142 (11.972; 35.706)	18.864 (15.935; 20.364)
Undulating exocuticle					
<i>S. vulgatum</i>	2.820 (2.477; 3.693)	5.104 (4.441; 6.290)	–	–	–
<i>M. b. basilaris</i>	2.791 (2.323; 3.361)	4.337 (3.536; 5.632)	15.087 (6.137; 18.607)	9.706 (8.676; 11.674)	–
Endocuticle					
<i>S. vulgatum</i>	55.935 (53.586; 57.800)	67.022 (64.618; 68.802)	–	31.307 (25.090; 34.743)	–
<i>M. b. basilaris</i>	69.758 (67.236; 73.803)	69.542 (61.410; 73.977)	36.696 (34.212; 42.158)	27.058 (19.421; 38.039)	–
Mixed cuticle					
<i>S. vulgatum</i>	16.343 (14.162; 18.752)**	21.370 (19.917; 22.835)**	–	–	–
<i>M. b. basilaris</i>	–	–	–	–	–

*Mesocuticle: sum of cross sectional thickness of dorsal and ventral membrane halves.

**In case a mixed cuticle is present, its thickness value has to be subtracted from the one of the endocuticle. The thickness of the latter decreases in favor of the mixed cuticle.

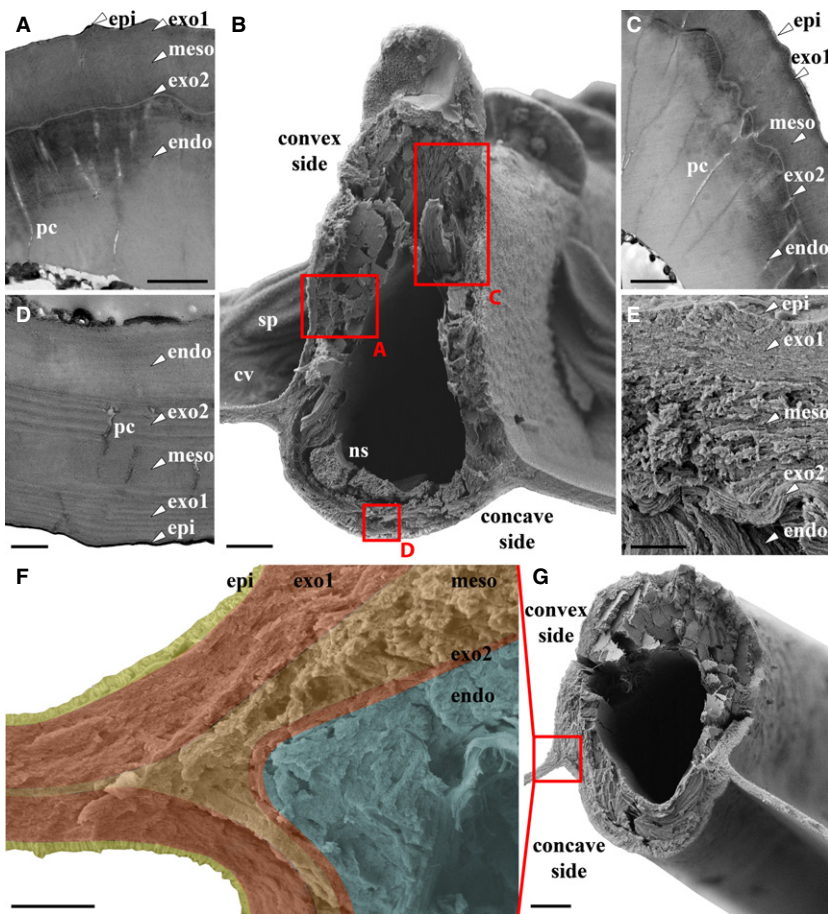


Fig. 3 *Matrona basilaris basilaris* (MBB) and *Sympetrum vulgatum* (SV), cuticle layers in longitudinal veins. (A–D) MBB, longitudinal vein cross-section. (A, C, D) TEM images, lateral side (A), convex side (C) and concave side (D) of the longitudinal cross-section (indicated by the red squares A, C and D), comprising the first five cuticle layers. (B) SEM image, overview of the longitudinal vein cross-section. (E–G) SV, longitudinal vein. (E) Outer part of the concave side cuticle layer, showing the first five cuticle layers. (F) Detail of (G) (indicated by the red square), showing the arrangement of the first five cuticle layers at the transition from longitudinal vein to membrane. endo, endocuticle; epi, epicuticle; exo1, outer exocuticle; exo2, undulating exocuticle; meso, mesocuticle; ns, nanospheres; pc, pore channel. Scale bars: 2 μm (A, C, E, F); 6 μm (B); 0.5 μm (D); 8 μm (G).

rarely, spheres of larger diameter ($0.52 \pm 0.09 \mu\text{m}$) were found in longitudinal veins of SV.

The inner cavity of longitudinal veins was filled with haemolymph and tracheae. Most probably nerves can also be found, though they were not detected in this study. In most cases, one single trachea occupied from one-third up to one-half of the inner cavity [Fig. 4D,G (trachea coloured in yellow)]. This trachea, however, was often found to be subdivided by leaf-like protrusions, sometimes forming subcavities (Fig. 4D,J, see sd). In most of the veins, the trachea was found to engage the concave side of the vein's inner cavity (Fig. 4D), whereas in others it was found in the central or side regions of the cavity (Fig. 4G). Main tracheae did not show the typical circumferential thickenings (taenidia). Instead, underlying cytoplasmic projections or microtrichia, named tubercles or punctuate thickenings (Locke, 1957; Richards & Richards, 1979; Mill, 1998), were found on the internal membrane of the tracheae (Fig. 4H,J). They had an average diameter of $0.14 \pm 0.02 \mu\text{m}$.

Although veins were cryofixed, that part of the vein that was supposed to contain haemolymph often showed only haemolymph remains sticking to the inner basal lamina of the epidermal cells or to the cuticle layers (Fig. 4G).

Cross veins of SV also showed an inner cavity, but only in the case of very thick cross veins, as the ones joined to ScP,

tracheae and haemolymph were found. In the majority of the cross veins examined, the inner cavity was empty. In contrast, the inner cavity of the majority of cross veins of MBB was almost completely filled with nanospheres (Fig. 5B,D), and no tracheae or haemolymph were discernible. Additionally, the central part of these cross veins showed two dark coloured, electron-dense protrusions (secondary stiffening elements), protruding at the level of the wing membrane, and almost touching each other, thus dividing the cross vein cavity into an upper and lower half (Fig. 5B,D).

Cuticular structure of veins and the wing membrane. Longitudinal veins. Longitudinal veins showed the full set of up to six different cuticle layers, the epicuticle, the outer exocuticle, the mesocuticle, the undulating exocuticle, the endocuticle, and the mixed cuticle or a set of five different cuticle layers with the mixed cuticle lacking (Figs 2A–C, 3A–E and 6A,D). The mixed cuticle was usually missing in longitudinal veins of MBB (Figs 2A and 3A–D), whereas wings of SV had either five or six cuticle layers (Figs 2B, 3G and 4G). The total thickness of the cuticle and the relative thickness of every single cuticle layer differed between the longitudinal vein's convex and concave sides. Median thickness and percentiles of every single cuticle

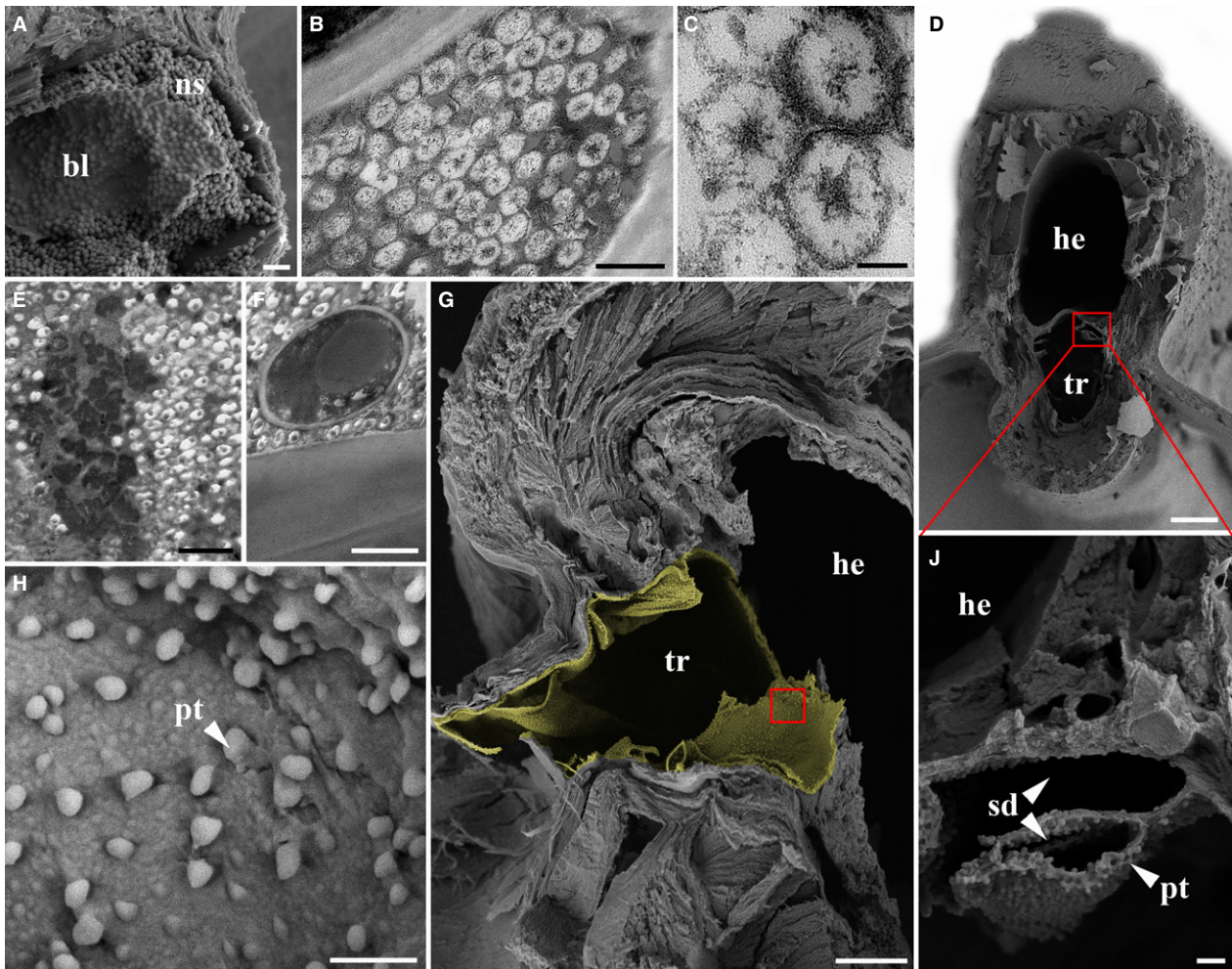


Fig. 4 *Matrona basilaris basilaris* (MBB) and *Sympetrum vulgatum* (SV) wing vein epidermis and cavity. (A, D, G, H, J) SEM images, vein cross-sections in MBB (A) and in SV (D, G, H, J). (B, C, E, F) TEM images. (A) Nanospheres (ns) with underlying basal lamina (bl). (B) Cross vein cross-section filled with nanospheres. (C) Detail of (B), showing nanospheres with the dark inner central spot. (D) Longitudinal vein (RA) cross-section, showing the typical division of the inner cavity with the haemolymph cavity on the convex vein side and the trachea on the concave side. (E, F) Electron-dense inclusions, probably pigments embedded in nanospheres. (G) Longitudinal vein cross-section with trachea (tr, coloured in yellow) on the vein's side and partly separated haemolymph-filled cavity (he). (H) Detail of (G), indicated by a red square, showing punctuate thickenings (pt) of the inner tracheal membrane. (J) Detail of (D), indicated by the red square, showing tracheal protrusions forming trachea subdivisions. bs, basal lamina; he, haemolymph-filled cavity; ns, nanospheres; pt, punctuate thickenings; sd, tracheal subdivision; tr, trachea. Scale bars: 1 μm (A, E, F); 100 nm (C); 10 μm (D); 5 μm (G); 500 nm (B, H, J).

layer are shown in Table 1. In general, the convex side had a thickness of 11.77 (8.56; 14.52) μm (median, 25th percentile; 75th percentile) in MBB and of 21.50 (18.47; 25.38) μm in SV. The concave side had a thickness of 3.42 (3.03; 3.96) μm or 7.28 (6.07; 11.86) μm in MBB, depending on whether the wing side exhibited a whitish blue colouration or not, and a thickness of 13.78 (11.50; 15.48) μm in SV. With about 50–75% for both convex and concave sides of both odonate species, the endocuticle occupied the largest part of the longitudinal vein cross-section of both longitudinal veins of both species studied (Figs 3A,C and 6A,D; Table 1). Comparative statistical analyses are discussed in the following section.

Transition vein to membrane. As can be seen in Figs 3F and 5D, only the epicuticle, the outer exocuticle and a thinning part of the mesocuticle constitute the actual part of the transition zone, and were further found in the membrane. The other cuticle layers, including the undulating exocuticle and the endocuticle, typically showed only a slight bending towards the transition zone. The proportion of the mesocuticle decreased towards the wing membrane.

Membrane. The wing membrane was shown to consist of three cuticle layers, the epicuticle, the exocuticle and the mesocuticle (Figs 6C,F and 7A–D). In the wing membrane of SV, though, the mesocuticle is often reduced to an almost invisible layer (Fig. 7B,D). In the proximal part of SV wings,

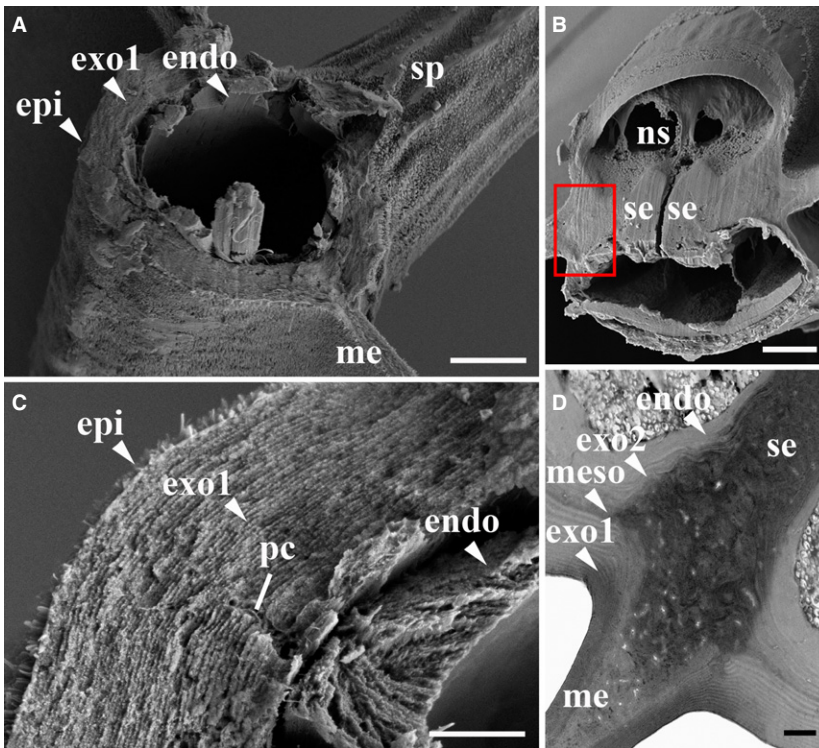


Fig. 5 *Sympetrum vulgatum* (SV) and *Matrona basilaris basilaris* (MBB), cuticle layers in cross veins. (A–C) SEM images. (D) TEM image. (A, C) SV. (A) Cross vein fracture showing a reduced number of only three cuticle layers. (C) Detail of (A). (B, D) MBB. (B) Cross vein cross-section. (D) TEM image of the transition region indicated by the red square in (B), showing five different cuticle layers. endo, endocuticle; epi, epicuticle; exo1, outer exocuticle; exo2, undulating exocuticle; me, wing membrane; meso, mesocuticle; ns, nanospheres; pc, pore channel; se, central stiffening element; sp, spine. Scale bars: 5 µm (A, B); 1 µm (C, D).

the wing membrane had a median thickness of 4.31 (4.16; 4.48) µm, whereas in wings of MBB it had a mean thickness of 1.64 (1.38; 1.81) µm. In both species, the exocuticle took up the largest part of the membrane cross-section with 82.89 (81.63; 83.56) % in SV wings and 58.06 (55.65; 60.14) % in MBB wings (see Table 1). The other part consisted of both epicuticle and mesocuticle, with the epicuticle occupying a slightly larger part (Table 1).

Cross veins. Cross veins usually had a round cross-section with a constant cuticle thickness (Fig. 6B,E). The number of cuticle layers differed between cross veins of both species studied. In MBB wings they had a set of five different cuticle layers, comparable to those of longitudinal veins (Fig. 5B,D). In contrast, SV cross veins typically showed a reduced set of three cuticle layers, namely the epicuticle, the exocuticle and the endocuticle (Fig. 5A,C). Exceptions of this arrangement included the so-called bracket-like ScP cross veins, located in the proximal part of the leading edge region in SV wings. Their structure, thickness distribution and the set of five cuticle layers strongly resembled the one of longitudinal veins. Cross veins of MBB had a median cuticle thickness of 3.97 (3.10; 4.32) µm. In SV wings, they had a median cuticle thickness of 4.15 (3.48; 4.52) µm. With 63.40 (59.55; 65.86) % in SV wings and 29.28 (14.90; 45.76) % in MBB wings, the exocuticle was found to be the most prominent layer in the cross vein cuticle.

Relative thickness of cuticle layers in longitudinal veins, cross veins and the wing membrane. SV. Comparison of the longitudinal vein sides. The statistical comparison of the

convex side and the concave side of longitudinal veins revealed a significant difference in their total cuticle thicknesses ($P < 0.001$). The cuticle thickness of the concave side was shown to be smaller than that of the convex side. Differences in single layer proportions were most prominent in the mesocuticle, undulating exocuticle and endocuticle (all $P < 0.001$). The mesocuticle proportion was much higher on the convex side, whereas the proportions of undulating cuticle and endocuticle were smaller. In contrast, epicuticle and exocuticle proportions showed only slight differences ($P = 0.015$, SV-epicuticle; $P < 0.001$, SV-exocuticle; see Table 1), both showing slightly higher values on the convex side. In those longitudinal veins, which additionally had a mixed cuticle, the endocuticle was shown to have a significantly smaller relative thickness. More or less exactly this portion, however, was covered by the mixed cuticle. Thus, endocuticle and mixed cuticle together made up the same portion as the endocuticle in veins with only five layers and without the mixed cuticle.

Comparison of longitudinal veins and cross veins. In SV wings, cross veins showed only three different layers, the epicuticle, the outer exocuticle and the endocuticle. Thus, there was no possibility for direct comparison. Therefore, the following two different approaches were taken. First, the relative cuticle layer thicknesses were directly compared by focusing only on the three main cuticle layers (epicuticle, outer exocuticle and endocuticle). Second, the relative thicknesses for outer exocuticle, mesocuticle and undulating exocuticle were combined, and these three layers were considered as one.

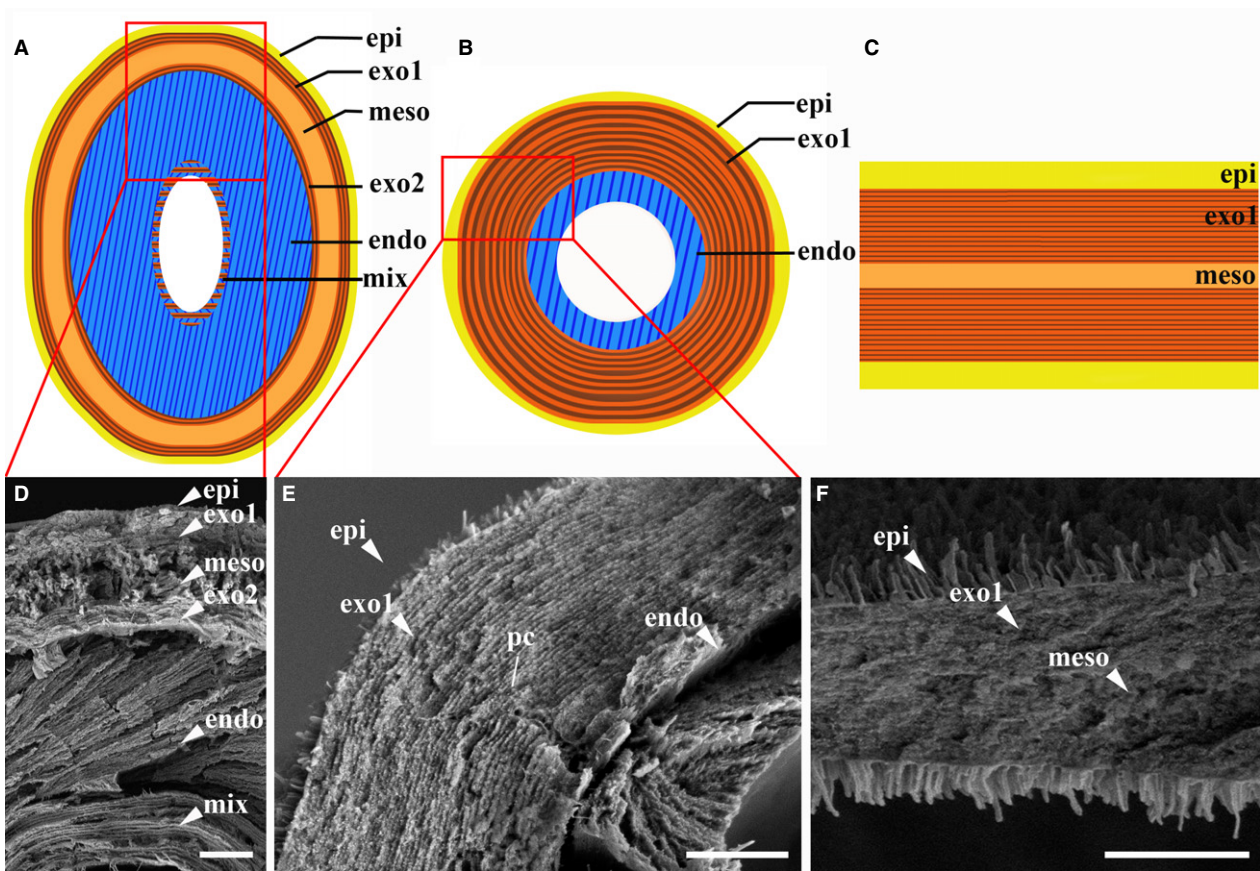


Fig. 6 *Matrona basilaris basilaris* (MBB) and *Sympetrum vulgatum* (SV), longitudinal vein, cross vein and wing membrane structure. (A–C) Model of cuticle structure in longitudinal vein (A), cross vein (B) and membrane (C). (D–F) SEM images. (D, E) Longitudinal vein (D) and cross vein (E) cross-sections of wings of SV. (F) Wing membrane cross-section of MBB wing. endo, endocuticle; epi, epicuticle; exo1, outer exocuticle; exo2, undulating exocuticle; meso, mesocuticle; mix, mixed cuticle; pc, pore channel. Scale bars: 2 μm (D); 1 μm (E, F).

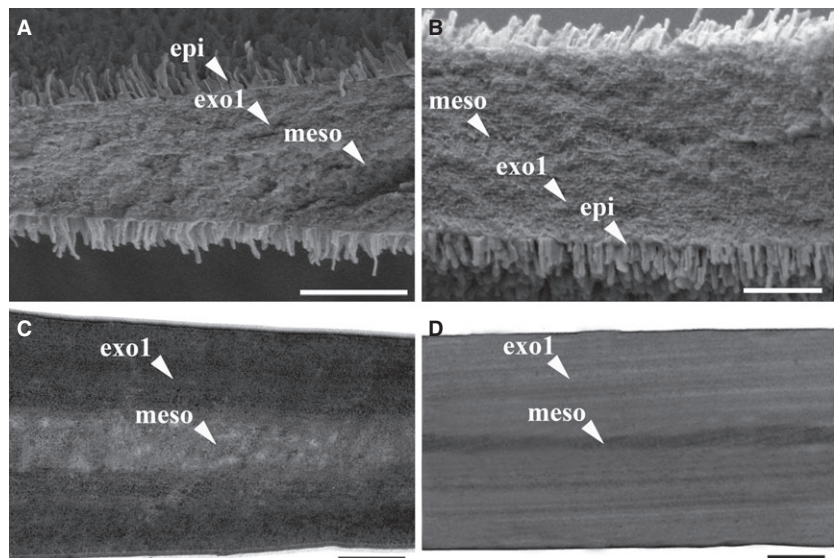


Fig. 7 *Matrona basilaris basilaris* (MBB) and *Sympetrum vulgatum* (SV), cuticle layers of the wing membrane. (A, C) MBB, membrane cross-section. (B, D) SV, membrane cross-section. (A, B) SEM images. (C, D) TEM images. epi, epicuticle; exo1, outer exocuticle; meso, mesocuticle. Scale bars: 1 μm (A, D); 500 nm (B, C).

Both approaches showed statistically significant differences ($P < 0.001$) of the cuticle thicknesses of the whole cuticle and the single cuticle layers between the convex side of

longitudinal veins and the cross vein cuticle. The analyses revealed that cross veins have a much smaller relative endocuticle thickness (see Table 1), whereas that of the exocuti-

cle is more than five times larger. In contrast, the endocuticle of the convex side of longitudinal veins covered more than 50%. Thus, it may be concluded that, in cross veins, the exocuticle covered a comparatively higher proportion (even when including the relative thickness of mesocuticle and undulating exocuticle), whereas the endocuticle had a smaller relative thickness than in longitudinal veins.

Consistent results were achieved for the comparison of the concave side of longitudinal veins with cross veins. Statistical analyses showed a significant difference in both total cuticle thickness and relative thickness of the single cuticle layers ($P < 0.001$). The only exception was the even larger proportion of the endocuticle in the cuticle of the concave side of longitudinal veins.

MBB. Comparison of longitudinal vein sides. Wings of MBB showed brownish and whitish-blue coloured wing veins. In general, the whitish-blue colouration was associated with the concave wing vein side. In the following text, non-reflecting (brownish) and reflecting (whitish-blue coloured) vein sides are referred to. In this part, the differences between the non-reflecting convex side, the non-reflecting concave side and the reflecting concave side are reported on.

The comparison of the total cuticle thickness of the convex side and concave side of non-reflecting longitudinal veins revealed that the concave side is significantly smaller than the convex side ($P < 0.001$), but that there is only a slight difference in the single cuticle layer proportions ($P = 0.004$, endocuticle; $P < 0.001$, epicuticle, exocuticle, mesocuticle, undulating exocuticle). However, considering the very small difference in actual epicuticle thickness, the difference in relative epicuticle thickness is mainly due the different total cuticle thicknesses.

The comparison of the convex side with the reflecting concave side showed that the cuticle thickness of the reflecting concave side is much smaller than that of the convex side ($P < 0.001$), and that, in contrast to the non-reflecting concave side, the proportional values for the cuticle layers also differ significantly ($P < 0.001$).

Further, the cuticle thickness of the reflecting concave side of longitudinal veins was shown to be significantly smaller than that of non-reflecting concave sides ($P < 0.001$). As expected from comparisons with the convex side, cuticle proportions of all layers were significantly different in non-reflecting and reflecting longitudinal concave sides. Here, the cuticle of the reflecting concave side showed a significantly lower proportion of the endocuticle ($P < 0.001$), but a particularly high proportion of both the outer exocuticle and undulating exocuticle ($P < 0.001$).

Comparison of longitudinal veins and cross veins. The comparison of the cuticle of the longitudinal vein convex side, non-reflecting concave side and reflecting concave side with the reflecting cross vein cuticle revealed some interesting correlations. Whereas the cuticle thickness of

the longitudinal vein convex side and non-reflecting concave side were found to be much larger than that of cross veins, the cuticle thickness of the reflecting concave side was shown to be almost identical with the cuticle thickness of cross veins. Even more, statistical analyses showed no significant difference in mesocuticle ($P = 0.059$), and only a slight, but significant difference in epicuticle and undulating exocuticle portions ($P = 0.001$). Exocuticle and endocuticle portions, however, differed significantly. In cross veins, the exocuticle portion was higher ($P < 0.001$), whereas the endocuticle portion was smaller ($P < 0.001$) than in the reflecting concave side cuticle of longitudinal veins. Convex side and non-reflecting concave side showed significant differences to cross veins in total cuticle thickness as well as in single cuticle layer thicknesses ($P < 0.001$; see Table 1).

Comparison of the cuticle layer thicknesses in both odonate species. Comparison of longitudinal vein sides. The comparison of the longitudinal vein convex sides in wings of both odonate species revealed significant differences in both total cuticle thickness ($P < 0.001$) and relative thickness of the single cuticle layers ($P < 0.001$). The median cuticle thickness of the longitudinal vein convex side in SV wings was found to be almost twice as large as in MBB wings. The main differences in the relative thickness of the single cuticle layers were found in the outer exocuticle, mesocuticle and endocuticle, with the outer exocuticle and mesocuticle being larger and the endocuticle being smaller in SV wings. The relative thickness of the epicuticle was shown to be slightly higher on the convex side of longitudinal veins of MBB ($P < 0.001$). The comparison of the undulating cuticle showed a very small difference between the species ($P = 0.003$).

Comparing the relative thickness of the non-reflecting concave side of longitudinal MBB veins and the concave side of SV revealed only a slightly significant difference in mesocuticle ($P = 0.002$) and endocuticle portions ($P = 0.005$). The undulating exocuticle was shown to have a significantly larger relative thickness in SV wings ($P < 0.001$). The relative thickness of the epicuticle was found to be significantly smaller and the outer exocuticle to be significantly larger in longitudinal veins of SV ($P < 0.001$). As already stated for the comparison of the total thickness of the longitudinal vein convex sides, the concave side of the longitudinal veins of SV was significantly larger than in MBB wings ($P < 0.001$).

In contrast to the cuticle of the non-reflecting concave side, that of the reflecting concave side showed significant and really pronounced differences in the total cuticle thickness and the relative thickness of the single layers ($P < 0.001$). As in previous comparisons, the total cuticle thickness was much higher in SV wings ($P < 0.001$). In contrast to the comparison with the non-reflecting concave side, where only a slight difference was found, here the endocuticle showed a much higher relative thickness in longitudinal veins of SV ($P < 0.001$). Epicuticle, outer exocuticle,

mesocuticle and undulating cuticle were all found to be smaller in SV wings ($P < 0.001$).

Comparison of cross veins. As already stated above, SV cross veins had only three different cuticle layers, including the epicuticle, the outer exocuticle and the endocuticle. Cross veins of MBB had a set of five cuticle layers, including the epicuticle, the outer exocuticle, the mesocuticle, the undulating exocuticle and the endocuticle. For comparison, the same approaches used for comparing the longitudinal cuticle and cross vein cuticle of SV were followed. When combining the relative thicknesses of the outer exocuticle, the mesocuticle and the undulating exocuticle of cross veins of MBB, statistical analysis showed only a small difference in the relative thickness of the epicuticle ($P < 0.001$), but a larger difference in the outer exocuticle (in MBB the combination of three cuticle layers) and the endocuticle, with cross veins of MBB having a smaller relative thickness of the endocuticle and a higher proportional thickness of the exocuticle, even though consisting of a combination of three cuticle layers. The total cuticle thickness of cross veins showed a slightly larger cuticle thickness in SV ($P < 0.001$).

Comparison of membranes. Wing membranes of both species had only three different cuticle layers, the epicuticle, the outer exocuticle and the mesocuticle. In the proximal part of the wing, the wing membrane of SV was found to be twice as thick as that of MBB ($P < 0.001$). Additionally, the SV wing membrane was shown to have a significantly higher portion of exocuticle ($P < 0.001$) and a much smaller portion of mesocuticle ($P < 0.001$).

Fluorescence microscopy

Resilin was previously shown to have an autofluorescence at the narrow band of wavelengths at about 415 nm when excited with UV-light (about 320 nm; Andersen & Weis-Fogh, 1964; Andersen, 2003; Burrows et al. 2008). Nevertheless, Michels & Gorb (2012) revealed that resilin can be successfully visualised by using CLSM in combination with a 405-nm laser. Both methods were used and revealed the presence of resilin in the endocuticle of wing veins of both species studied (Fig. 8A,C,D,F). In contrast to the endocuticle of longitudinal veins, which showed a strong blue autofluorescence (Fig. 8A,C), the endocuticle of cross veins showed a comparatively weak blue and a rather strong green autofluorescence (Fig. 8G), when using the same laser intensity and gain.

Michels & Gorb (2012) additionally showed that CLSM is appropriate for visualising different cuticle compositions, for example, the degree of sclerotisation. Based on these assumptions, the deep red autofluorescence of the outer and the undulating exocuticles of the longitudinal wing veins of SV may suggest a higher degree of sclerotisation as in the orange fluorescing mesocuticle (Fig. 8A). The endocuticle was found to be dominated by blue autofluorescence but, additionally, revealed the existence of a green-yellowish fluorescing transition zone in its outermost part,

directly underlying the undulating cuticle (Fig. 8A,C). The latter varies in its thickness and the degree of dominance of green-yellowish fluorescence. The analyses of longitudinal veins of MBB showed comparable results, though the presence of a dark brown pigment in part of the endocuticle and the undulating exocuticle made the interpretation difficult (Fig. 8D,F, see pi).

Interestingly, the fluorescence microscopical analyses additionally revealed that dorsal and ventral vein sides not only differ in their thickness, but also in their material composition (Fig. 8A,C,D,F). Here, the concave side of longitudinal veins showed a strong green autofluorescence in SV wing veins instead of the typical red autofluorescence, indicating a lower degree of sclerotisation (Fig. 8A,C; in addition to the previously mentioned overall reduced thickness of cuticle layers). This difference is also present and especially intriguing in MBB wing veins as all cuticle layers of reflecting vein sides were shown to be unsclerotised, virtually transparent showing a bright blue autofluorescence (Fig. 8E,F). Non-reflecting longitudinal veins, in contrast, showed only negligible differences in single cuticle layer autofluorescences (Fig. 8E,D). Possible effects on structural colouration will be discussed below. Comparable to reflecting vein sides of longitudinal veins of MBB, cross veins showed a bright blue autofluorescence in all cuticle layers (Fig. 8H,I).

Another interesting fact is that a bright blue autofluorescence in the wing membrane was found. This blue autofluorescence, however, is restricted to those parts of the wing membrane located directly next to the wing veins (Fig. 8A, B), including both cross and longitudinal veins. Thus, especially in the proximal part of the wing, veins seemed to be suspended in a resilin-bearing membrane.

LM

To verify the current assumptions based on the results of fluorescence microscopical analyses, different staining methods were used, namely the Heidenhain's azan staining, Cason's staining, toluidine blue staining and Nile blue staining.

Azan staining. Azan staining allows differentiating between sclerotised and non-sclerotised cuticle (Richards, 1967; Dettner & Peters, 2003; Dirks & Dürr, 2011). In SV veins, the unsclerotised endocuticle stained blue, whereas the sclerotised outer exocuticle and the undulating exocuticle stained dark red to orange (Fig. 9A). The mesocuticle showed a bright red colour (Fig. 9A). The phenomenon of cuticle being refractory to staining was previously shown to be due to strong sclerotisation (Blaney & Chapman, 1969), and was often found in parts of the outer exocuticle (Fig. 9A).

Cason's staining. Cason's staining allows differentiating between resilin-bearing cuticle and sclerotised cuticle.

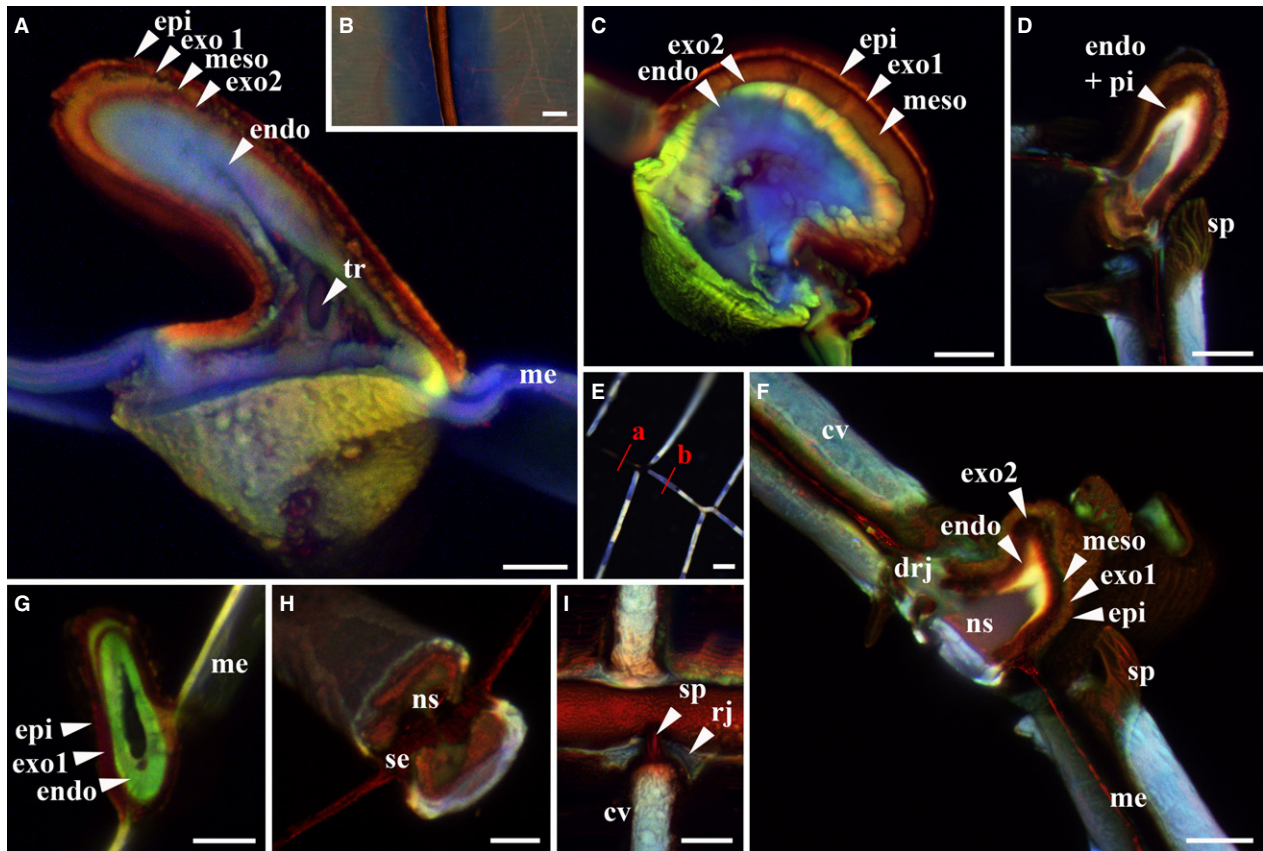


Fig. 8 *Sympetrum vulgatum* (SV) and *Matrona basilaris basilaris* (MBB), fluorescence microscopy. (A–D, F–I) CLSM images. (E) FLM image. (A, B, C, G) SV. (D–F, H, I) MBB. (A, B) ScP cross vein and adjacent blue fluorescing membrane. (A) Cross-section. (B) ScP convex side. (C) Cross-section of MA longitudinal vein. (G) Cross-section of a cross vein. (D) Non-reflecting longitudinal vein. (E) Longitudinal vein and adjacent cross veins, a and b indicating cutting sides for (D, F). (F) Single-side reflecting longitudinal vein showing blue autofluorescence on the reflecting concave side. (H) Cross vein showing nanospheres (ns) and the central stiffening element (se). (I) Cross veins connected to the longitudinal vein in the form of resilin- and spine-bearing wing vein joints. cv, cross vein; drj, double-sided resilin-bearing wing vein joint; endo, endocuticle; epi, epicuticle; exo1, outer exocuticle; exo2, undulating exocuticle; me, wing membrane; meso, mesocuticle; ns, nanospheres; pi, pigment; rj, resilin-bearing wing vein joint; se, central stiffening element; sp, spine; tr, trachea. Scale bars: 10 μ m (A, G, H); 50 μ m (B, E); 20 μ m (C, D, F, I).

Previous studies showed that resilin is stained violet to pink in its pure form, and blue when co-occurring with chitin microfibrils (Cason, 1950; Romeis, 1989; Jäkle 2003). Sclerotised cuticle, in contrast, stains yellow to brown and transitional cuticle of a lower degree of sclerotisation red. In this study, the outer exocuticle and undulating exocuticle of longitudinal veins were shown to stain yellow-brown, whereas the mesocuticle stained red and the endocuticle blue, indicating the coexistence of resilin and chitin microfibrils (Fig. 9C).

Toluidine blue staining. Toluidine blue stains basophilic structures and was previously shown to be one of the criteria indicating the presence of rubberlike cuticle (resilin) by a sapphire to bright blue colour (Weis-Fogh, 1960). In contrast, solid cuticle does not stain at all (Weis-Fogh, 1960). After staining, only the endocuticle showed the typical blue colour (Fig. 9B). In MBB wings, though, the colour was shifted to indigo-violet (Fig. 10B,E,F). This phenomenon is

commonly known as metachromasia and may be assigned to the high abundance of carboxyl groups in melanin (Schubert & Hamerman, 1956; Bergeron & Singer, 1958; Myers et al. 2008).

Nile blue staining. A dark brown pigment was found to be homogeneously deposited in a distinct part of the cuticle of MBB wing veins. Examinations of unstained sections revealed areas of brown appearance primarily located in the endocuticle and the undulating exocuticle (Fig. 10A). These areas showed no sharp outline, but rather a continuous transition into the otherwise colourless region of the endocuticle. In the majority of MBB veins, the very central and inner parts of the cross-sections were devoid of pigments. Bleaching and subsequent staining of the vein cross-sections with Nile blue confirmed the presence of melanin in the endocuticle in the form of a greenish colour (Fig. 10D). The presence of melanin in insect wings or scales has already been reported from various insect

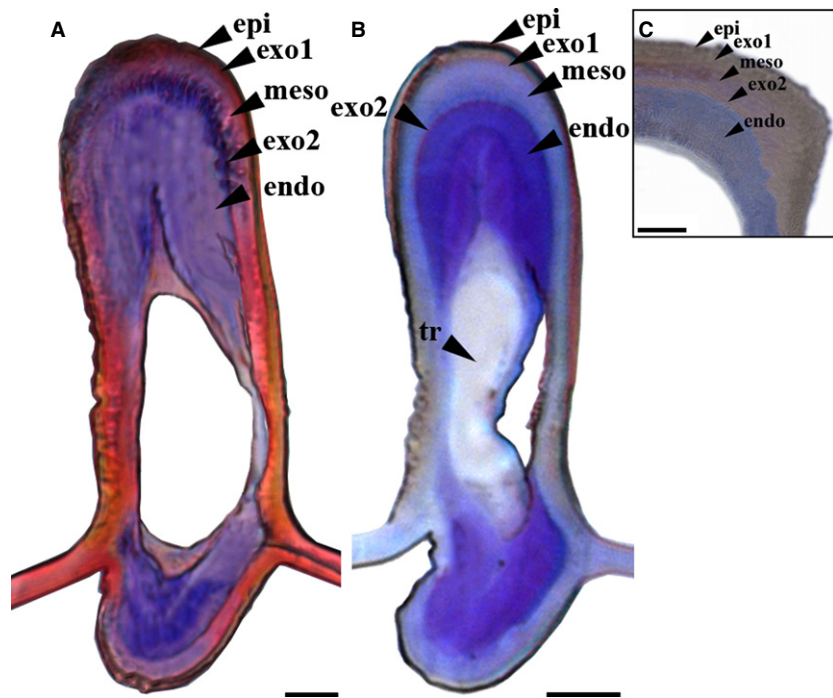


Fig. 9 *Sympetrum vulgatum*, LM, stained sections. (A, B) ScP cross vein. (A) Cross-section stained with Heidenhain's azan stain. (B) Cross-section stained with toluidine blue. (C) Part of the longitudinal vein cross-section stained with Cason's stain. endo, endocuticle; epi, epicuticle; exo1, outer exocuticle; exo2, undulating exocuticle; meso, mesocuticle; tr, trachea. Scale bars: 10 µm.

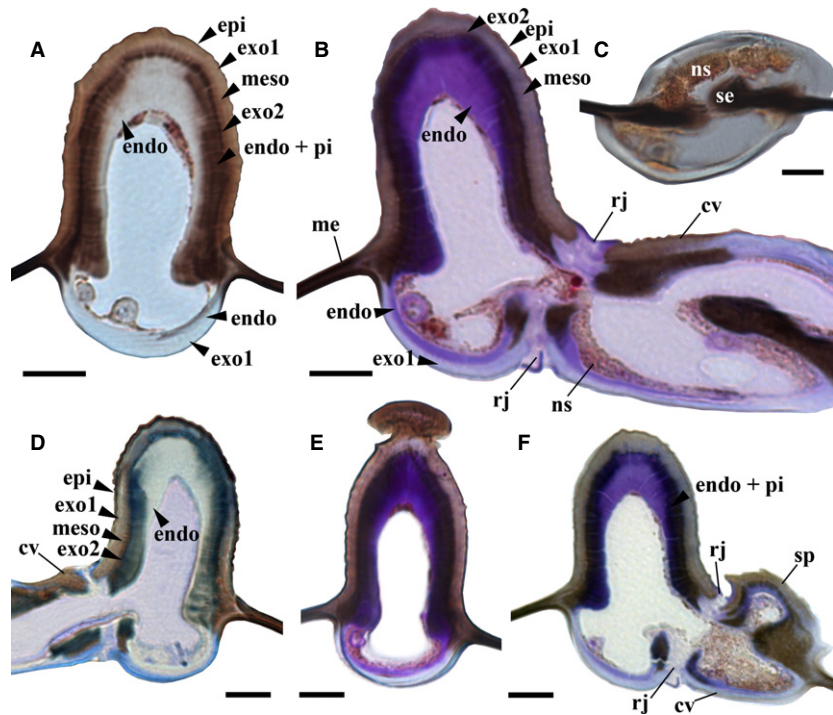


Fig. 10 *Matrona basilaris basilaris*, LM, stained sections. (A, B, D–F) Cross-sections of a reflecting longitudinal vein with adjacent wing membrane or cross vein. (C) Cross-section of the reflecting cross vein. (A) Unstained section showing the presence of melanin in the endocuticle and undulating exocuticle. (B, E, F) Sections stained with toluidine blue showing the presence of resilin in the endocuticle of longitudinal and cross veins and in wing vein joints. (C) Unstained cross-section showing nanospheres. (D) Section bleached and stained with Nile blue showing the presence of melanin (greenish colour). cv, cross vein; endo, endocuticle; epi, epicuticle; exo1, outer exocuticle; exo2, undulating exocuticle; me, wing membrane; meso, mesocuticle; ns, nanospheres; pi, pigment; rj, resilin-bearing wing vein joint; se, central stiffening element; sp, spine; tr, trachea. Scale bars: 20 µm (A, B, D–F); 10 µm (C).

species, including representatives of Lepidoptera and Odonata (Corbet, 1999; Stavenga et al. 2004; Hooper et al. 2006).

Reflectance measurements

In order to determine the exact hue (wavelength of the peak at the highest reflectance) and the brightness/

intensity [the reflectance (%) in this peak] of the wing vein colouration of MBB, wavelengths between 300 and 800 nm were recorded, including the UV and infrared part of the spectrum. As shown in Fig. 11, the hue with a brightness of $7.58 \pm 1.76\%$ ($n = 5$) reflectance was recorded at a wavelength of 436.67 ± 5.89 nm ($n = 5$), corresponding to the blue colouration of the wing veins.

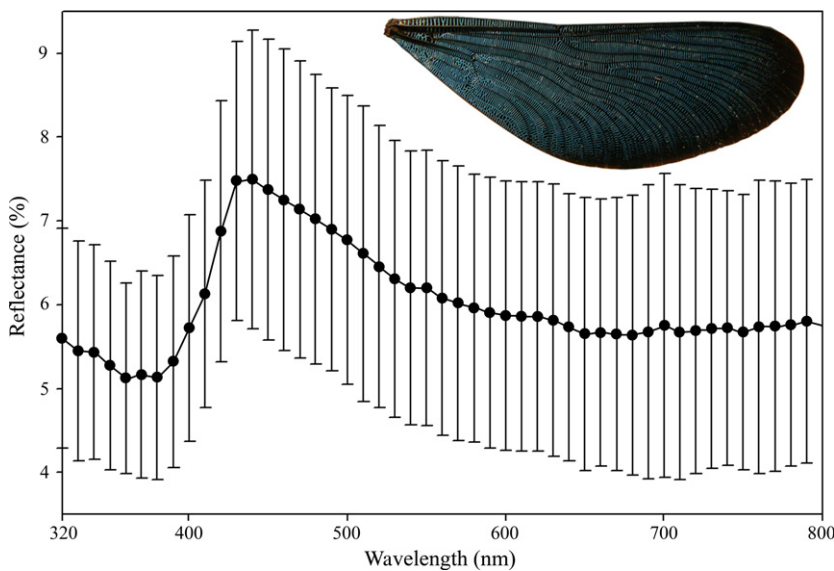


Fig. 11 *Matrona basilaris basilaris*, mean of reflectance measurements of cut out and tightly arranged wing veins showing a whitish-blue colouration. The hue is at the range of wavelengths of 430–440 nm.

Discussion

Load conditions of beam-like elements with different cross-sections and possible failure mechanisms

Different cases of elastic deformation such as bending, buckling and torsion of beam-like elements are defined in Fig. 12, and may resemble the basic load cases of natural veins. Figure 12 shows exemplarily bending of a beam with single fixed support (A) under an applied load F (Eq. 1), buckling with different boundary conditions (B, Eq. 2) and torsion under a torsional moment M (C, Eq. 3). The product $E \cdot I$ in Eqs 1 and 2 is the bending stiffness and stiffness against buckling, whereas $G \cdot I$ in Eq. 3 is the torsional stiffness, with E being the Young's modulus and G the shear modulus. The second moment of inertia I depends on the cross-section of the beam, and is also shown for some simple cross-sections in Fig. 12.

Natural veins, however, are composed of different co-axially layered materials (see Fig. 6) with different material properties and potentially different interfacial properties between the layers. Furthermore, it is known that some layers contain highly oriented fibres that presumably lead to anisotropic material properties and may lead to direction-dependent mechanical response under different load cases.

However, as a first approximation one may characterise the mechanical response of natural veins by replacing the product $E \cdot I$ and $G \cdot I$, respectively, in Eqs 1–3 by the sum of, for example, the bending stiffnesses of individual layers $\sum E_i I_i$ (Wienss, 2008).

¹So far, only elastic deformations were considered, and failure or plastic deformations have been neglected. In Fig. 13, different types of failures of long and thin-walled tubes (Dirks & Taylor, 2012) are shown that may also apply to the current case of natural veins. Failure may either occur by fracture when local stresses (either tensile, compressive

or shear) reach the strength of the corresponding material [Fig. 13(1)] or by (local) buckling that leads to irreversible plastic deformations of the material [Fig. 13(2a, 2b)]. Furthermore, there is another buckling instability in long thin-walled tubes subjected to bending that arises from the ovalisation of the cross-section [Brazier 1927; Dirks & Taylor, 2012; Fig. 13(2c)], that is a bended tube with initially circular cross-section becomes elliptical. Finally, the splitting of such tubes may be another type of failure [Fig. 13(3); Dirks & Taylor, 2012].

Moreover, failure may generally occur by the interaction between the above-described failure mechanisms depending on the specific material and geometrical properties and on the specific load case (Dirks & Taylor, 2012).

Possible functions of resilin-bearing sandwich-like structure of the wing vein

Because wing veins also have a transporting function, they are of tube-like shape and bear a channel inside that is filled with trachea, haemolymph and nerves. During flight, this tube-like construction of wing veins is subjected to elastic deformations, including bending, buckling and torsion, and runs the risk to overbend, fracture or deform irreversibly. Depending on their dimensions and overall linkage to surrounding veins and the wing membrane, cross and longitudinal veins are subjected to different amounts of bending, buckling and torsional deformations.

Recent studies showed that cross veins are flexibly joined to longitudinal veins in the form of resilin-bearing wing vein joints, thereby contributing to an increased chord-wise flexibility or lower flexural stiffness, which is advantageous for passively performed wing deformations (Appel & Gorb, 2011; Donoughe et al. 2011). Longitudinal veins, in contrast, have much lower possibility to yield to bending, buckling and torsional loads with the help of flexible joints.

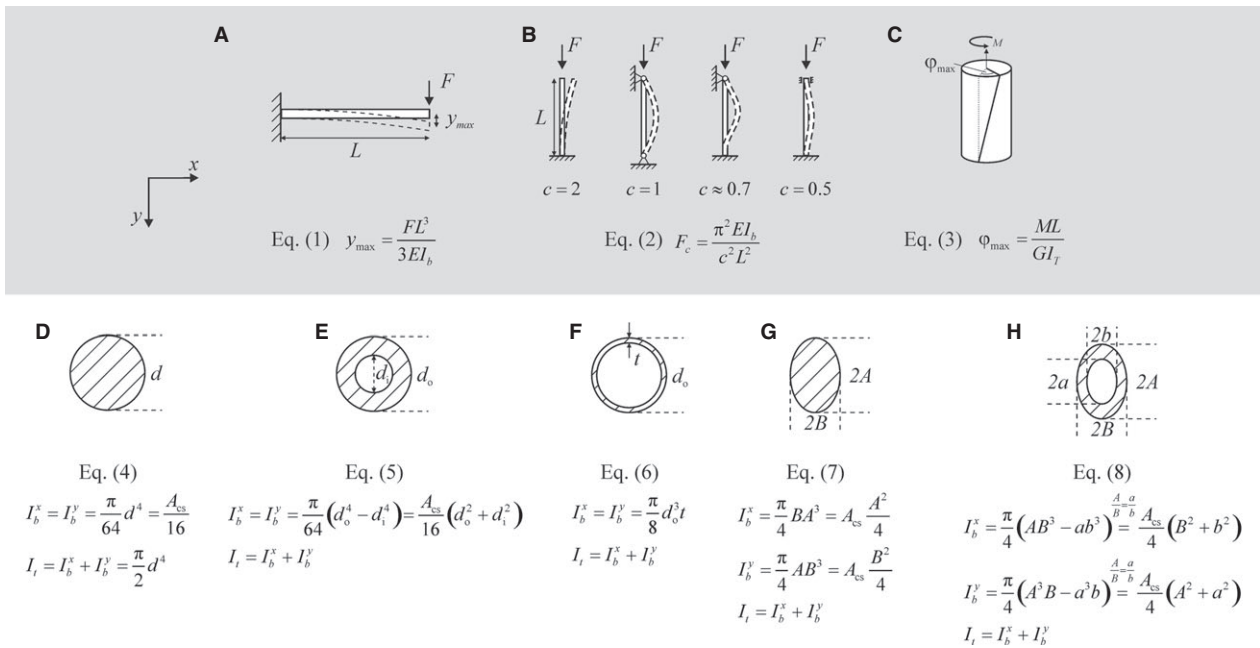


Fig. 12 Load conditions of beam-like elements with different cross-sections. (A–C) Equations of possible elastic deformations: (A) bending; (B) buckling; and (C) torsion (Holzmann et al. 2012). (D–H) Schemes for different cross-sections with corresponding equations of second moment of inertia for bending, buckling and torsion (4) – (8). A, length semi-major axis of ellipse; a, length of semi-major axis of inner ellipse diameter; A_{cs} , area cross-section; B, length semi-minor axis of ellipse; b, length semi-minor axis of inner ellipse diameter; d_o , outer diameter; d_i , inner diameter; E, Young’s modulus; F, applied force; G, shear modulus; I, second moment of inertia; L, length; M, torsional moment; t, width of thin circular ring; y, deflection (bending); c, effective buckling length factor ($c = 0.5$ for both column ends fixed, $c = 1$ for both column ends pinned, free rotation, $c \approx 0.7$ for one end fixed and one end pinned, $c = 2$ for one end fixed and the other free), ϕ , torsion.

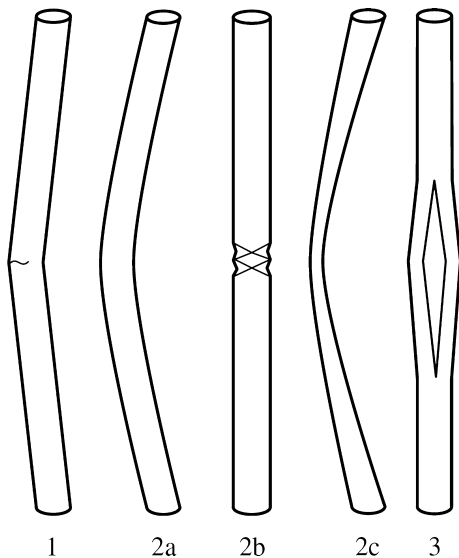


Fig. 13 Different possible elastic/plastic failure modes of long, thin-walled tubes. 1, fracture; 2a, Euler buckling; 2b, local buckling; 2c, buckling by ovalisation; 3, splitting (Dirks & Taylor, 2012).

In this study, it was found that wing veins consist of up to six different cuticle layers, showing distinctive structural and compositional and, thus most probably, mechanical differences. The arrangement of cuticle layers and their

material composition suggest the presence of a stiffness gradient decreasing towards the vein’s interior, with the hard, sclerotised exocuticle as an outer shell, and an inner core layer consisting of the soft and compliant, resilin-dominated endocuticle. This gradient is further sophisticated through the existence of a transitional zone, consisting of mesocuticle and undulating exocuticle, found in longitudinal veins of both species examined and in MBB cross veins. Such a gradient with smooth transition in composition across the interface was assumed to improve interfacial bonding between dissimilar materials (Suresh, 2001), and may thus improve the structure’s stability.

The principle of improving the load-carrying capacity (the ratio of load bearing to weight; and to counteract Brazier ovalisation) by using composite materials with a thin-walled hard cylindrical shell, supported by a compliant soft core, has already been described for, for example, plant stems, porcupine quills or hedgehog spines (Karam & Gibson, 1994). The stronger ability of such constructions to bear higher buckling loads under uniaxial compression or pure bending than that of equivalent hollow shells with the same weight but without softness gradient was shown in various studies (Hutchinson & He, 2000; Barlga & Rotherth, 2002; Ma et al. 2008). Whereas in the previously mentioned examples, the thin-walled cylindrical structures are often supported by a honeycomb or foam-like cellular core, in

wing veins of dragonflies and damselflies, the compliant core or layer is seemingly represented by the resilin-bearing endocuticle.

Based on the data of Mises stress distribution and the flexural deformation analysis using the finite element analysis, Chen et al. (2012) further concluded that the maximum bending stress of such a hollow 'hard shell-soft core' or sandwich-design model of the diameter of wing veins is mainly maintained by the outer stiffer layer. This is in accordance with the study of Giannakopoulos & Suresh (1997), who, by developing a general theory for frictionless normal indentation of elastically graded materials by point loads, could predict that in the case of a decreasing elastic modulus the peak value of local tensile stresses is moved closer to the surface. This, in turn, is in agreement with the general assumption that the strongest elements, here most probably the exocuticle, are located in regions that experience the highest stresses (e.g. in bamboo, plant stems and bones; Suresh, 2001). Further, according to Wang et al. (2008), the torsional deformation of a sandwich-like structured wing vein was found to mainly occur at the inner layer under axial torque. Additionally, circumferentially aligned chitin fibres in the compliant, soft layer were suggested to contribute to the absorption of the torsional deformation (Chen et al. 2012) and may, thus, serve as inner support, improving the tensile strength.

Variation of these properties may arise from differences in cross-sectional shape, cuticle thickness and composition of single layers. As mentioned in the section 'Load conditions of beam-like elements with different cross-sections and possible failure mechanisms', bending, buckling and torsional stiffnesses of layered veins may be approximated by the sum of all respective stiffnesses (thus, being also related to their cross-sectional proportion).

In contrast to longitudinal veins, cross veins are short and were found to have a rather round cross-section, a significantly thicker exocuticle and less blue autofluorescence in their endocuticle. In elliptically shaped longitudinal veins, the endocuticle was found to constitute a much larger part of the vein cross-section and to be dominated by resilin. Thus, it may be assumed that cross veins (especially those of SV) have a stiffer endocuticle and a less pronounced softness gradient than longitudinal veins. Their shortness, together with the probably relatively high stiffness, may reduce elastic deformations at a given load. Resilin-dominated wing vein joints provide cross veins with a flexible linkage to longitudinal veins and may, thereby, reduce failure of cross veins and enable chordwise wing deformations.

In longitudinal veins, flexible joints are lacking. Thus, a failsafe against permanent damage has to be provided by the vein itself. In the case of longitudinal veins, their high slenderness, the existence of a composite material with a hard shell and a more compliant, resilin-bearing core may increase elastic deformations at a given load. For a detailed analysis of the load-bearing capacity of wing veins, i.e. the

failure load for a given failure type, detailed information about the material and interfacial properties of individual layers and layer connections is necessary. Nevertheless, two facts may be found that might prevent or at least increase the load-bearing capacity against failure by ovalisation. Although longitudinal veins are long and hollow cylindrical elements, they are filled with haemolymph that provides a certain resistance against the change in cross-sectional shape. Moreover, longitudinal veins have ellipse-like cross-sections, with the long axis coinciding with the direction of the flapping wing (Dirks & Taylor, 2012). This may further delay ovalisation as the cross-section during bending would become first more circular (Dirks & Taylor, 2012) before elliptical again, but now with the long axis perpendicular to the direction of bending.

Comparing the thickness of wing veins in SV and MBB, it was found that longitudinal veins of SV have a much larger total cuticle thickness than longitudinal veins of MBB, especially on their convex sides, with particularly the exocuticle and the mesocuticle being larger. Considering the higher density of longitudinal and especially cross veins in wings of MBB, it might be suggested that the larger thickness and probably stiffness may reduce elastic deformations and may outbalance the reduced amount of rigidity imparting veins in wings of SV. This may also be related to the higher wing loading, higher wing beat frequency and higher flight velocity of anisopteran species (Rüppell, 1989). The much larger thickness of the wing membrane in wings of SV may also be attributed to this fact. Additional studies are necessary to further elucidate this issue.

Based on the present study and previous literature data, functional significance of such a heterogeneous material composition as found in wing veins of SV and MBB may be assumed, arising from a stiff, tanned and dehydrated exocuticle and a soft, compliant inner layer (endocuticle) with rather circumferentially aligned chitin-fibres. (i) This kind of structure reduces the overall stiffness of veins, individually depending on the proportion of single cuticle layers and, thereby, may influence the amount of elastic deformations at a given load. (ii) Elastic energy storage is enhanced due to the low stiffness and high resilience of such structures (Weis-Fogh, 1960, 1961a,b), especially in veins with a large resilin-dominated endocuticle. (iii) Ovalisation, primarily in elliptically shaped, haemolymph-filled longitudinal veins, with the sclerotised outer cuticle probably providing stability against inflation, is presumably delayed. (iv) The gradient of material properties contributes to the protection of the fragile structures in the inner cavity of the wing vein, such as tracheae and nerves. However, to prove these hypotheses, local mechanical measurements are required in the future.

Wing membrane

The network of longitudinal and cross veins is interconnected through thin membranous areas. The latter mainly

consist of exocuticle and a thin layer of mesocuticle, arranged in a sandwich-like manner (Fig. 7A–D). The current results indicated that the cuticle composition shows significant differences between the wing membrane directly abutting on the vein and that located in the middle of such a wing membrane area or cell. The wing membrane located next to the veins was dominated by blue autofluorescence, indicating the high concentration of resilin in these areas (Fig. 8A,B). Such a flexible suspension may help preventing the veins to tear off from the wing membrane, allowing a larger range of elastic deformations and a lesser probability of the stress concentration at the site of membrane suspension to the vein.

Vein colouration

In this study, the presence of nanospheres underlying the cuticle of longitudinal veins and almost entirely filling the cross vein cavities in MBB wings were also described. As illustrated in Figs 3B,D, 5B,D, 8F,H and 10A–F, the presence of nanospheres was always correlated with a transparent or translucent, unsclerotised and often resilin-bearing cuticle of small thickness, and also with the production of a blue colour in daylight. The presence of nanospheres in epidermal cells underlying the cuticle has already been described for abdominal tergites of dragonflies and damselflies (Veron et al. 1974; Prum et al. 2004). Their connection to structural colouration was first proposed by Mason in (1926) and in more detail by Veron et al. in (1974), who suggested these non-iridescent structural blue colours to be produced by incoherent Tyndall or Raleigh scattering. This hypothesis, ascribing the blue structural colouration of insects to incoherent light scattering, has been abided for many years (Fox, 1976; Charles & Robinson, 1981; Parker, 1999), until a study by Prum et al. (2004) showed that the recorded reflectance spectra lack the inverse fourth power relationship predicted for incoherent Raleigh scattering. Instead, they proposed to attribute the structural blue colouration to coherent light scattering of quasioordered arrays (here consisting of nanospheres), lacking the production of prominent iridescence (Prum et al. 1998, 1999, 2004; Prum & Torres, 2003a). Reflectance spectra of abdominal tergites of *Enallagma civile* (Hagen, 1861) and *Anax junius* Drury, 1773 revealed a hue at 460 and 475 nm (Prum et al. 2004). This hue wavelength in the latter study was longer than the one measured in the current study, revealing a peak wavelength at about 430–440 nm, thus showing a different shade of blue. The reflectance spectra recorded of abdominal tergites of *Anax junius*, however, also showed reflectance peaks at 430–440 nm (Prum et al. 2004). Whether this difference in wavelength may be correlated to a different structure or size of nanospheres or overlying cuticle is unclear, because shrinkage/swelling of nanospheres during different electron microscopy procedures cannot be completely excluded. An interesting fact,

however, which was discussed for the plumage colour of Steller's jays, is that a basal melanin layer, underlying the nanostructured spongy layer, responsible for the structural blue colouration of their feathers, may function to absorb incoherently scattered white light, thereby increasing the purity of the blue colour (Shawkey & Hill, 2006). In MBB wings, melanin was found in the endocuticle and undulating exocuticle of longitudinal veins (Fig. 10A,B,D–F, see pi), and in the form of strongly dark pigmented, electron-dense, central stiffening elements in cross veins (Figs 5B,D, 8H and 10C, see se). In the first case, melanin may dominantly suppress colouration, whereas in the latter, these central dark pigmented elements, which are absent in SV cross veins, may have an effect comparable to the one in Steller's jay feathers.

To conclude, it has been suggested that the blue colouration of MBB wing veins is produced by coherent scattering of nanospheres underlying a thin, unsclerotised cuticle. This blue colouration may probably be enhanced by the presence of underlying pigments, especially distinct in cross veins in the form of strongly dark pigmented central stiffening elements, emanating from the wing membrane. The lack of colouration, which was often observed on the convex side of longitudinal veins, in contrast, is probably due to the overall large cuticle thickness, the strong pigmentation of the endocuticle and undulating exocuticle, as well as due to the high degree of sclerotisation in the exocuticle.

Conclusion

Taking into account that insect wings lack internal wing muscles, their aerodynamic performance strongly depends on passive deformations. Previous studies showed that flexible wing vein joints endow the dragonfly wing with increased chordwise flexibility, thereby influencing directional wing deformations during flight. It was previously reported that the presence of resilin in insect wings in the form of flexible, resilin-bearing wing vein joints serves to support passive wing deformations. As shown in this study, the combination of varying cuticle thickness, cross-sectional shape and stiffness gradient, supported by the presence of resilin in the internal cuticle layers, may also influence the extent of elastic deformation of wing veins and thereby most likely improve their resistance to failure under mechanical load.

It has been shown that the wing vein cuticle consists of up to six different cuticle layers, and that longitudinal and cross veins differ significantly in relative thickness of exo- and endocuticle, with cross veins showing a much thicker exocuticle. Cuticle layers show structural and compositional differences (in the degree of sclerotisation and the occurrence of resilin), suggesting a stiffness gradient decreasing towards the vein's interior, which is especially pronounced in longitudinal veins. This composite construction may be assumed to reduce the overall vein stiffness, thereby

influencing the extent of elastic deformations at a given load, to enhance elastic energy storage, and to delay ovalisation, especially important for the highly stressed longitudinal veins. In contrast, cross veins show a less pronounced stiffness gradient, are shorter and probably stiffer than longitudinal veins. Here, flexible, resilin-bearing vein joints may act as a failsafe against permanent damage. Further local measurements are needed to prove the suggested hypotheses. Additionally, the degree of vein cuticle sclerotisation and melanisation were correlated to the occurrence of nanospheres, which are responsible for the structural blue colouration of some wing veins of MBB.

Acknowledgements

The authors would like to thank Prof. Dr K. Krupinska and Dr M. Mulisch (Central Microscopy Unit, Center of Biology, Kiel University, Germany) for providing access to the transmission electron microscope. This work was supported by the Studienstiftung des Deutschen Volkes to EA.

References

- Andersen SO (1963) Characterization of a new type of cross-linkage in resilin, a rubber-like protein. *Biochim Biophys Acta* **69**, 249–262.
- Andersen SO (2003) Structure and function of resilin. In: *Elastomeric Proteins: Structures, Biomechanical Properties and Biological Roles*. (eds Schwery P, Tatham AS, Bailey AJ), pp. 259–278. New York: Cambridge University Press.
- Andersen SO (2010) Studies on resilin-like gene products in insects. *Insect Biochem Mol Biol* **40**, 541–551.
- Andersen SO, Weis-Fogh T (1964) Resilin. A rubberlike protein in arthropod cuticle. *Adv Insect Physiol* **2**, 1–65.
- Appel E, Gorb SN (2011) Resilin-bearing wing vein joints in the dragonfly *Epiophlebia superstes*. *Bioinspir Biomim* **6**, 046006.
- Azuma A, Watanabe T (1988) Flight performance of a dragonfly. *J Exp Biol* **137**, 221–252.
- Banerjee S (1988) Organization of wing cuticle in *Locusta migratoria* Linnaeus, *Tropidacris cristata* Linnaeus and *Romalea microptera* Beauvais (Orthoptera: Acrididae). *Int J Insect Morphol Embryol* **17**, 313–326.
- Barbakadze N, Enders S, Gorb SN, et al. (2006) Local mechanical properties of the head articulation cuticle in *Pachnoda marginata* (Coleoptera, Scarabaeidae). *J Exp Biol* **209**, 722–730.
- Barlga S, Rothert H (2002) An idealization concept for the stability analysis of ring-reinforced cylindrical shells under external pressure. *Int J Nonlinear Mech* **37**, 745–756.
- Bennet-Clark HC, Lucey ECA (1976) The jump of the flea: a study of the energetic and a model of the mechanisms. *J Exp Biol* **47**, 59–76.
- Bergeron JA, Singer M (1958) Metachromasy: an experimental and theoretical reevaluation. *J Biophys Biochem Cytol* **4**, 433.
- Binnington K, Retnakaran A (1991) Epidermis – a biologically active target for metabolic inhibitors. In: *Physiology of the Insect Epidermis*. (eds Binnington K, Retnakaran A), pp. 307–334. Australia Melbourne: CSIRO.
- Blaney WM, Chapman RF (1969) The fine structure of the terminal sensilla on the maxillary palps of *Schistocerca gregaria* (Forsskål) (Orthoptera, Acrididae). *Z Zellforsch Mikrosk Anat* **99**, 74–97.
- Brazier LG (1927) On the flexure of thin cylindrical shells and other ‘thin’ sections. *Proc R Soc Lond A* **116**, 104–114.
- Burrows M, Shaw SR, Sutton GP (2008) Resilin and chitinous cuticle form a composite structure for energy storage in jumping by froghopper insects. *BMC Biol* **6**, 41.
- Cason JE (1950) A rapid one-step Mallory-Heidenhain stain for connective tissue. *Stain Technol* **25**, 225–226.
- Chapman RF (1998) *The Insects: Structure and Function*, pp. 441–477. Cambridge, UK ; New York : Cambridge University Press.
- Charles MS, Robinson JV (1981) A scanning electron microscope study of the blue reflecting particles in *Enallagma civile* (Hagen) (Zygoptera: Coenagrionidae). *Odonatologica* **10**, 219–222.
- Chen Y, Wang X, Ren H, et al. (2012) Hierarchical dragonfly wing: microstructure-biomechanical behavior relations. *J Biomech Eng* **9**, 185–191.
- Combes SA, Daniel TL (2001) Shape, flapping and flexion: wing and fin design for forward flight. *J Exp Biol* **204**, 2073–2085.
- Combes SA, Daniel TL (2003) Flexural stiffness in insect wings. I. Scaling and the influence of wing venation. *J Exp Biol* **206**, 2979–2987.
- Corbet PS (1999) *Dragonflies, Behaviour and Ecology of Odonata*. Ithaca, NY: Cornell University Press.
- Dettner K, Peters W (2003) *Lehrbuch der Entomologie*. p. 9. München: Spektrum Akademischer, Elsevier GmbH.
- Dirks J-H, Dürr V (2011) Biomechanics of the stick insect antenna: damping properties and structural correlates of the cuticle. *J Mech Behav Biomed Mater* **4**, 2031–2042.
- Dirks J-H, Taylor D (2012) Veins improve fracture toughness of insect wings. *PLoS ONE* **7**, e43411.
- Donoughe S, Crall JD, Merz RA, et al. (2011) Resilin in dragonfly and damselfly wings and its implications for wing flexibility. *J Morphol* **272**, 1409–1421.
- Du G, Sun M (2010) Effects of wing deformation on aerodynamic forces in hovering hoverflies. *J Exp Biol* **213**, 2273–2283.
- Elvin CM, Carr AG, Huson MG, et al. (2005) Synthesis and properties of crosslinked recombinant pro-resilin. *Nature* **437**, 999–1002.
- Fox DL (1976) *Animal Biochromes and Structural Colors*. Berkeley, CA: University of California Press.
- Fujimori E (1978) Blue-fluorescent bovine α -crystallin. *Biochem Biophys Acta* **534**, 82–88.
- Garcia-Castineiras S, Dillon J, Spector A (1978) Non-tryptophan fluorescence associated with human lens protein; apparent complexity and isolation of bityrosine and anthranilic acid. *Exp Eye Res* **26**, 461–476.
- Gast R, Lee J (1978) Isolation of the *in vivo* emitter in bacterial bioluminescence. *Proc Natl Acad Sci USA* **75**, 833–837.
- Giannakopoulos AE, Suresh S (1997) Indentation of solids with gradients in elastic properties: part I. Point force. *Int J Solids Struct* **34**, 2357–2392.
- Gorb SN (1999) Serial elastic elements in the damselfly wing: mobile vein joints contain resilin. *Naturwissenschaften* **86**, 552–555.
- Holzmann G, Meyer H, Schumpich G, et al. (2012) *Technische Mechanik Festigkeitslehre*. Wiesbaden: Vieweg+Teubner.
- Hooper IR, Vucusic P, Wootton RJ (2006) Detailed optical study of the transparent wing membranes of the dragonfly *Aeshna cyanea*. *Opt Express* **14**, 4891–4897.
- Hutchinson JW, He MY (2000) Buckling of cylindrical sandwich shells with metal foam cores. *Int J Solids Struct* **37**, 6777–6794.

- Jäkle B (2003) Resilin in insect flight systems. Diploma thesis, University of Tübingen pp. 11–12, 31.
- Jongerius SR, Lentink D (2010) Structural analysis of a dragonfly wing. *Exp Mech* **50**, 1323–1334.
- Karam GN, Gibson LJ (1994) Biomimicking of animal quills and plant stems: natural cylindrical shells with foam cores. *Mater Sci Eng, C* **2**, 113–132.
- Kim W-K, Ko JH, Park HC, et al. (2009) Effects of corrugation of the dragonfly wing on gliding performance. *J Theor Biol* **260**, 523–530.
- Koehler C, Liang Z, Gaston Z, et al. (2012) 3D reconstruction and analysis of wing deformation in free-flying dragonflies. *J Exp Biol* **215**, 3018–3027.
- Kuitunen K, Gorb SN (2011) Effects of cuticle structure and crystalline wax coverage on the coloration in young and old males of *Calopteryx splendens* and *Calopteryx virgo*. *Zoology* **114**, 129–139.
- Kukalová-Peck J (1974) Wing-folding in the paleozoic insect order Diaphanopteroidea (Paleoptera), with a description of new representatives of the family Elmoidae. *Psyche* **81**, 315–333.
- Lentink D, Jongerius SR, Bradshaw NL (2009) The scalable design of flapping micro-air vehicles inspired by insect flight. In: *Flying Insects and Robots*, Ch. 4. (eds Floreano D, Zufferey JC, Srinivasan MV, Ellington C), pp. 185–205. Berlin, Heidelberg: Springer.
- Locke M (1957) The structure of insect tracheae. *Q J Microsc Sci* **98**, 487–492.
- Ma J-F, Chen W-Y, Zhao L, et al. (2008) Elastic buckling of bionic cylindrical shells based on bamboo. *J Bionic Eng* **5**, 231–238.
- Mason CW (1926) Structural colors of insects. *J Phys Chem* **30**, 383–395.
- Maxwell MH (1978) Two rapid and simple methods used for the removal of resins from 1.0 μm thick epoxy sections. *J Microsc* **112**, 253–255.
- Michels J, Gorb SN (2012) Detailed three-dimensional visualization of resilin in the exoskeleton of arthropods using confocal laser scanning microscopy. *J Microsc* **245**, 1–16.
- Mill PJ (1998) Tracheae and tracheoles. In: *Microscopic Anatomy of Invertebrates*, 11A. (eds Harrison FW, Locke M), pp. 303–336. New York: Insecta, Wiley-Liss.
- Mountcastle AM, Combes SA (2013) Wing flexibility enhances load-lifting capacity in bumblebees. *Proc R Soc Lond B*, **280**, 20130531.
- Myers RB, Fredenburgh JL, Grizzle WE (2008) Carbohydrates. In: *Theory and Practice of Histological Techniques*. (eds Bancroft JD, Gamble M), pp. 178–179. Philadelphia, USA: Churchill Livingstone, Elsevier Science.
- Nachtigall W (1977) Zur Bedeutung der Reynoldszahl und der damit zusammenhängenden strömungsmechanischen Phänomene in der Schwimmphysiologie und Flugbiophysik. *Fortschr Zool* **24**, 13–56.
- Neville AC (1975) *Biology of the Arthropod Cuticle*. Berlin: Springer.
- Newman DJS (1982) The functional wing morphology of some Odonata. Ph.D. thesis, 281 pp, University of Exeter.
- Okamoto M, Yasuda K, Azuma A (1996) Aerodynamic characteristics of the wings and body of dragonfly. *J Exp Biol* **199**, 281–284.
- Parker AR (1999) Invertebrate structural colours. In: *Functional Morphology of the Invertebrate Skeleton*. (ed. Savazzi E), pp. 65–90. London: John Wiley.
- Pearse AGE (1964) *Histochemistry. Theoretical and Applied*. Boston: Little, Brown.
- Peisker H, Michels J, Gorb SN (2013) Evidence for a material gradient in the adhesive tarsal setae of the ladybird beetle *Coccinella septempunctata*. *Nat Commun* **4**, 1661.
- Prum RO, Torres RH (2003a) A Fourier tool for the analysis of coherent light scattering by bio-optical nanostructures. *Integr Comp Biol* **43**, 591–602.
- Prum RO, Torres RH (2003b) Structural colouration of avian skin: convergent evolution of coherently scattering dermal collagen arrays. *J Exp Biol* **206**, 2409–2429.
- Prum RO, Torres RH, Williamson S, et al. (1998) Coherent light scattering by blue feather barbs. *Nature* **396**, 28–29.
- Prum RO, Torres RH, Williamson S, et al. (1999) Two-dimensional Fourier analysis of the spongy medullary keratin of structurally coloured feather barbs. *Proc R Soc Lond B* **266**, 13–22.
- Prum RO, Cole JA, Torres RH (2004) Blue integumentary structural colours in dragonflies (Odonata) are not produced by incoherent Tyndall scattering. *J Exp Biol* **207**, 3999–4009.
- Prum RO, Quinn T, Torres RH (2005) Anatomically diverse butterfly scales produce structural colours by coherent scattering. *J Exp Biol* **209**, 748–765.
- Prum RO, Dufresne ER, Quinn T, et al. (2009) Development of colour-producing β -keratin nanostructures in avian feather barbs. *J R Soc Interface* **6**, 253–265.
- Qin G, Hu X, Cebe P, et al. (2012) Mechanism of resilin elasticity. *Nat Commun* **3**, 1003.
- Richards AG (1967) Sclerotization and the localization of brown and black colours in insects. *Zool Jahrb Abt Anat Ontogenie Tiere* **84**, 25–62.
- Richards AG, Richards A (1979) The cuticular protuberances of insects. *Int J Insect Morphol Embryol* **8**, 143–157.
- Romeis B (1989) Untersuchung des Binde- und Stützgewebes. In: *Mikroskopische Technik*, 17th edn. (ed. Böck P), pp. 501–502. München: Urban und Schwarzenberg.
- Romeis B (2010) chapter 3, Färbungen. In: *Mikroskopische Technik*. (eds Mulisch M, Welsch U), 18th edn, p. 209, 217–218. Heidelberg: Spektrum Akademischer.
- Rothschild M, Schlein J, Parker K, et al. (1975) The jumping mechanism of *Xenopsylla cheopsis*. *Philos Trans R Soc Lond B Biol Sci* **271**, 499–515.
- Rüppell G (1989) Kinematic analysis of symmetrical flight manoeuvres of Odonata. *J Exp Biol* **114**, 13–42.
- Sane SP (2003) The aerodynamics of insect flight. *J Exp Biol* **206**, 4191–4208.
- Schubert M, Hamerman D (1956) Metachromasia: chemical theory and histochemical use. *J Histochem Cytochem* **4**, 159–189.
- Shawkey MD, Hill GE (2006) Significance of a basal melanin layer to production of non-iridescent structural plumage color: evidence from an amelanotic Stellar's jay (*Cyanocitta stelleri*). *J Exp Biol* **209**, 1245–1250.
- Stanford BK, Kurdi M, Beran PS, et al. (2012) Shape, structure, and kinematic parameterization of a power-optimal hovering wing. *J Aircr* **49**, 1687–1699.
- Stavenga DG, Stowe S, Siebke K, et al. (2004) Butterfly wing colours: scale beads make white pierid wings brighter. *Proc R Soc Lond B* **271**, 1577–1584.
- Suresh S (2001) Graded materials for resistance to contact deformation and damage. *Science* **292**, 2247–2251.
- Vanella M, Fitzgerald T, Preidikman S, et al. (2009) Influence of flexibility on the aerodynamic performance of a hovering wing. *J Exp Biol* **212**, 95–105.

- Vargas A, Mittal R, Dong H** (2008) A computational study of the aerodynamic performance of a dragonfly wing section in gliding flight. *Bioinspir Biomim* **3**, 1–13.
- Veron JEN, O'Farrell AF, Dixon B** (1974) The fine structure of Odonata chromatophores. *Tissue Cell*, **6**, 613–626.
- Vincent JFV, Wegst UGK** (2004) Design and mechanical properties of insect cuticle. *Arthropod Struct Dev* **33**, 187–199.
- Vukusic P, Sambles JR** (2003a) Photonic structures in biology. *Nature* **424**, 852–855.
- Vukusic P, Wootton RJ, Sambles JR** (2003b) Remarkable iridescence in the hindwings of the damselfly *Neurobasis chinensis chinensis* (Linnaeus) (Zygoptera: Calopterygidae). *Proc R Soc Lond B* **271**, 595–601.
- Wakeling JM, Ellington CP** (1997) Dragonfly flight: I. Gliding flight and steady-state aerodynamics. *J Exp Biol* **200**, 543–556.
- Wang X, Li Y, Shi YF** (2008) Effects of sandwich microstructures on mechanical behaviours of dragonfly wing vein. *Compos Sci Technol* **68**, 186–192.
- Weis-Fogh T** (1960) A rubber-like protein in insect cuticle. *J Exp Biol* **37**, 889–907.
- Weis-Fogh T** (1961a) Thermodynamic properties of resilin, a rubber-like protein. *J Mol Biol* **3**, 520–531.
- Weis-Fogh T** (1961b) Molecular interpretation of the elasticity of resilin, a rubber-like protein. *J Mol Biol* **3**, 648–667.
- Wiens C** (2008) Simulation von Kabeln und Schläuchen – Anforderungen und Einflüsse. Ph.D. thesis, Koblenz-Landau University.
- Willkommen J** (2009) The tergal and pleural wing base sclerites – homologous within the basal branches of Pterygota? *Aquat Insects* **31**, 443–457.
- Wootton RJ** (1981) Support and deformability in insect wings. *J Zool (London)* **193**, 447–468.
- Wootton RJ** (1991) The functional morphology of the wings of Odonata. *Adv Odonatol* **5**, 153–169.
- Wootton RJ, Newman DJS** (2008) Evolution, diversification and mechanics of dragonfly wings. In: *Dragonflies and Damselflies. Model Organisms in Ecological and Evolutionary Research*, Chapter 20. (ed. Cordoba-Aguilar A), pp. 261–274. New York: Oxford University Press.
- Zhao L, Huang Q, Deng X, et al.** (2009) Aerodynamic effects of flexibility in flapping wings. *J R Soc Interface* **7**, 485–497.